Geological Society of America
Special Paper 378
2004

# *Siliciclastic record of rapid denudation in response to convergent-margin orogenesis, Ross Orogen, Antarctica*

**John W. Goodge***
*Department of Geological Sciences, University of Minnesota, Duluth, Minnesota 55812, USA*

**Paul Myrow**
*Department of Geology, Colorado College, Colorado Springs, Colorado 80903, USA*

**David Phillips***
*Research School of Earth Sciences, Australian National University, Canberra, ACT 0200, Australia*

**C. Mark Fanning**
**Ian S. Williams**
*Research School of Earth Sciences, Australian National University, Canberra, ACT 0200, Australia*

## ABSTRACT

**Siliciclastic rocks of the upper Byrd Group in the Transantarctic Mountains record rapid denudation and molasse deposition during Ross orogenesis along the early Paleozoic convergent margin of Gondwana. These rocks, which stratigraphically overlie Lower Cambrian Byrd carbonate deposits, are dominated by fresh detritus from proximal igneous and metamorphic sources within the Ross Orogen. Biostratigraphic evidence indicates that deposition of the siliciclastic succession is late Botomian or younger (<515 Ma). The largest modes of U-Pb and $^{40}Ar/^{39}Ar$ ages from detrital zircons and muscovites respectively in the siliciclastic molasse are Early to Middle Cambrian, but based on ages from crosscutting igneous bodies and neoblastic metamorphic phases, deposition of individual molasse units continued until ~490–485 Ma (earliest Ordovician). The entire episode of interrelated tectonic, denudational, sedimentary, deformational, and magmatic events is restricted to a time interval of 7–25 m.y. in the late Early Cambrian to earliest Ordovician, within the resolution of these stratigraphic and geochronologic data. Stratigraphic relationships suggest that the detrital zircon and muscovite in the sediments came from the same source terrain, consistent with large volumes of molasse having been shed into forearc and/or marginal basins at this time, primarily due to erosion of igneous rocks and metamorphic basement of the early Ross magmatic arc. Rapid erosion and unroofing in the axial Ross Orogen is consistent with a sharp carbonate-to-clastic stratigraphic transition observed in the upper Byrd Group, reflecting an outpouring of alluvial fan and fluvial-marine clastic detritus. The short time lag between tectonism and sedimentary response is similar to that determined for the corresponding section of the Ross-Delamerian orogen in South Australia and other continental-margin arc systems, such as in the Mesozoic Peninsular Ranges of California. Mineral cooling ages from metamorphic basement adjacent to the orogen yield a syn- to late-orogenic cooling**

*E-mail, Goodge: jgoodge@d.umn.edu. Current address, Phillips: School of Earth Sciences, University of Melbourne, Melbourne, VIC 3010 Australia.

Goodge, J.W., Myrow, P., Phillips, D., Fanning, C.M., and Williams, I.S., 2004, Siliciclastic record of rapid denudation in response to convergent-margin orogenesis, Ross Orogen, Antarctica, *in* Bernet, M., and Spiegel, C., eds., Detrital thermochronology—Provenance analysis, exhumation, and landscape evolution of mountain belts: Boulder, Colorado, Geological Society of America Special Paper 378, p. 105–126. For permission to copy, contact editing@geosociety.org.

**rate of ~10 °C/m.y., which, combined with a known metamorphic geotherm, indicates a denudation rate of ~0.5 mm/yr. Such denudation rates are comparable to those in recent convergent or collision orogens and suggest that crustal thickening associated with both magmatic intrusion and structural shortening was balanced by near-synchronous erosional exhumation.**

**Keywords:** detrital minerals, zircon, muscovite, thermochronology, Ross Orogen.

## INTRODUCTION

Thermochronology is widely used to recover information about cooling histories, metamorphic *P*-*T*-t paths, and rates of tectonic displacement. Differences between the ages of minerals with different closure temperatures, as well as mineral systems that record partial thermal resetting, can be used to determine crustal cooling rates. If the regional geothermal gradient is known or can be inferred, it is also possible to estimate the rate of surficial denudation. These methods are commonly applied to igneous and metamorphic rocks in tectonically active settings, sampled from bedrock across tilted crustal sections or in deeply eroded areas of high present-day relief. This approach has some limitations, however, due to the degree of relief and the fact that part of the rock record (thereby, history) has been removed by erosion. An alternative strategy is to determine the ages of detrital minerals eroded from a mountain belt and preserved by accumulation in adjacent sedimentary basins. Detrital mineral chronometers place limits on the age and duration of sedimentation, particularly when biostratigraphic markers are lacking. In some cases they can be used to estimate rates of cooling and/or denudation, if it can be demonstrated that minerals with different closure temperatures were derived from the same source region and that those minerals have not been isotopically disturbed in the surficial and burial environments since initial closure (e.g., Copeland and Harrison, 1990; Garver et al., 1999; Bernet et al., 2001). The latter situation most likely holds in proximal "unroofing" successions where mineral provenance is well established.

We have used detrital muscovite and zircon ages from Cambrian-Ordovician siliciclastic rocks of the central Ross Orogen (Fig. 1A) to evaluate tectonically induced denudation in a convergent-margin setting of Gondwana. Sandstone and conglomerate of the upper Byrd Group (Lower Cambrian to Ordovician) were deposited as forearc molasse sediments in response to structural shortening and continental-margin magmatism during the main phase of Ross tectonism (Rowell et al., 1988; Rees and Rowell, 1991). The onset of supracrustal deformation is well constrained by biostratigraphic, chemostratigraphic, and geochronological data from the region (Myrow et al., 2002b), and detrital mineral suites in the molasse deposits provide good control on their age and provenance (Goodge et al., 2002). Here we summarize previously reported U-Pb detrital zircon ages and report new $^{40}Ar/^{39}Ar$ detrital muscovite ages from the Byrd Group molasse succession that characterize the age and nature of inputs from the orogenic source region. Sandstone samples were collected for detrital zircon and muscovite analysis from the Starshot and Douglas formations between the Byrd and Beardmore glaciers (Fig. 2), near Cape Selbourne (DIF), Mount Ubique (USF), the Holyoake Range (HSF and DCS), Cambrian Bluff (CBG), Softbed Ridges (SRG) and Dolphin Spur (DSG). We also report new age measurements of crosscutting intrusions and metamorphic mineral assemblages that bracket the duration of molasse sedimentation. Taken together, these data provide a detailed record of interrelated events that followed the first pulse of supracrustal deformation in the region and that reflect rapid denudation in the orogen.

## GEOLOGICAL SETTING

East Antarctica is the keystone in most reconstructions of Rodinia and Gondwana. It has a long association with East Gondwana cratonic neighbors in present-day Australia, India, and Africa, which were finally amalgamated along Grenville-age sutures during assembly of Rodinia (Fig. 1A). Breakup of Rodinia resulted in formation of a rifted margin along the paleo-Pacific sector of Australia and East Antarctica (Fig. 1B), characterized by passive-margin subsidence, sedimentation in shoreline and shallow shelf settings, and minor volcanism (Laird, 1981, 1991; Stump, 1995; Preiss, 2000). Rifting along the East Antarctic sector may have occurred as early as ca. 750 Ma, but a gabbro from the central Transantarctic Mountains dated by U-Pb zircon as 668 Ma provides a better minimum estimate of rifting age (Goodge et al., 2002). Subsequent passive-margin extension and sedimentation continued well into the late Neoproterozoic between ca. 670 and 580 Ma. By the latest Neoproterozoic to Early Cambrian, the rift margin underwent a major tectonic transformation to an active, subducting plate boundary, probably as a result of changes in global plate motions and plate-boundary stresses following initial consolidation of the central Gondwana supercontinent (Flöttmann et al., 1994; Goodge, 1997).

In Antarctica, the convergent margin consisted of a continental-margin magmatic arc (Borg et al., 1987, 1990; Armienti et al., 1990; Allibone et al., 1993; Rocchi et al., 1997) constructed upon Archean-Proterozoic basement (Fig. 1C), with sinistral-oblique underflow interpreted from Ross-age basement structures (Goodge et al., 1993a). Calc-alkaline magmatism indicates that subduction was initiated by at least 530 Ma (e.g., Cox et al., 2000; Allibone and Wysoczanski, 2002). Detrital zircon geochronology from lower Paleozoic rocks containing arc-derived detritus suggests that volumetrically significant magmatism occurred as early as ca. 580 Ma (Ireland et al., 1998; Goodge et al., 2002). Tectonism attributed to the Ross Orogeny is expressed by structural shortening of upper Neoproterozoic marginal-basin

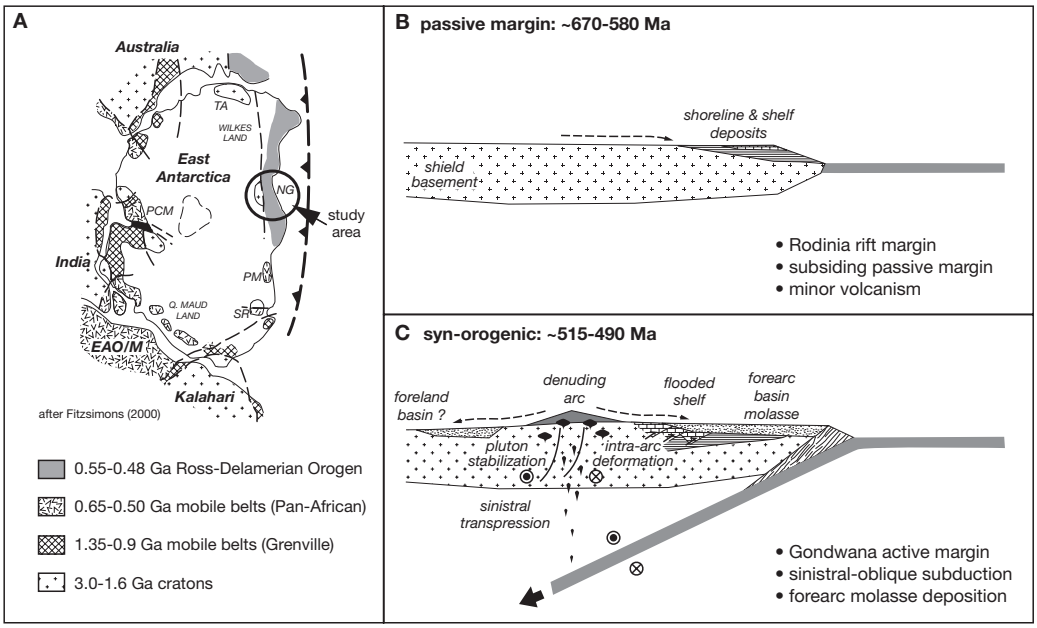


Figure 1. Tectonic setting of the Ross Orogenic belt. A: East Gondwana assembly (modified from Fitzsimons, 2000), showing distribution of major cratonic shield areas and Mesoproterozoic to Neoproterozoic mobile belts. General position of convergent plate margin during Ross-Delamerian stage shown by barbed line. Study area near Nimrod Glacier indicated by circle. EAO/M—East African Orogen/Mozambique Belt; NG—Nimrod Glacier area; PCM—Prince Charles Mountains; PM—Pensacola Mountains; SR—Shackleton Range; TA—Terre Adélie. B: Passive-margin setting of rifted East Antarctic shield in late Neoproterozoic time. This stage is represented stratigraphically by mature Beardmore Group siliciclastic rocks, deposited in shoreline and shelf settings (Myrow and Goodge, 1999), and minor mafic volcanic rocks dated at 668 Ma (Goodge et al., 2002). Passive-margin deposition continued to the middle Early Cambrian (up to 515 Ma) with deposition of platform carbonate deposits of the lower Byrd Group. C: Main orogenic phase of Ross convergent margin, characterized by sinistral-oblique subduction of paleo-Pacific oceanic lithosphere beneath the East Antarctic margin (Borg et al., 1990; Goodge et al., 1993a). Basement rocks of the Nimrod Group record deep-seated metamorphism, syntectonic magmatism, and deformation in a transpressional setting. Intra-arc deformation included shortening of older marginal-basin deposits and strike-slip motion within the developing magmatic arc. The main contractional orogenic phase within the supracrustal assemblages resulted in erosion of arc and arc-basement rocks, leading to alluvial fan, fluvial, and shoreline deposition of upper Byrd Group molasse materials in a forearc basin (Myrow et al., 2002b); the present-day polar ice cap flanks the denuded orogenic belt, but a foreland basin is conjecturally illustrated here.

strata and platform carbonates of Early Cambrian age. Middle Early Cambrian to Ordovician molasse deposits of the upper Byrd Group, the subject of this paper, appear to represent alluvial-fluvial to shallow-marine siliciclastic deposits derived from the eroding Ross Orogen (Rees and Rowell, 1991; Myrow et al., 2002a). As shown in Figure 1C, these deposits are interpreted as marginal-marine and forearc-basin sediments on the basis of paleocurrent and sedimentary facies data. There may have been a corresponding foreland basin in a retroarc setting, but if it existed, the deposits would now be covered by the modern ice cap.

In the central Transantarctic Mountains (Fig. 2), siliciclastic rocks of the upper Byrd Group lie east (or outboard in present coordinates) of high-grade metamorphic and igneous rocks of the Nimrod Group, representing East Antarctic shield basement and low-grade sedimentary rocks of the passive margin. The latter include late Neoproterozoic siliciclastic rocks of the Beardmore Group (following Goodge et al., 2002) and Early Cambrian carbonate strata of the lower Byrd Group (Fig. 3). The Beardmore Group deposits include quartz wacke, quartzite, carbonate grainstone, shale, diamictite, and minor mafic volcanic rocks. The Shackleton Limestone of the lower Byrd Group includes a thick basal quartz arenite unit. Siliciclastic rocks of middle Early Cambrian or younger age (Holyoake, Starshot, and Douglas formations of the upper Byrd Group) abruptly overlie the older passive-margin units (Myrow et al., 2002b). These rocks depositionally overlie the terminal Lower Cambrian carbonate platform deposits of the Shackleton Limestone and reflect tectonic drowning of the formerly quiescent platform during the early stages of Ross convergence. Faunal ages in the Holyoake and lower Starshot formations (lower part of the upper Byrd Group) date the inception of siliciclastic deposition as ca. 515 Ma (Myrow et al., 2002b). The bulk of the upper Byrd Group consists of proximal conglomerate and more distal sandstone, the latter being mainly immature feldspathic arenite and wacke associated with shale, argillite, and pebble conglomerate. Although difficult to distinguish from the older clastic rocks in the field, they are distinctive in composition, being notably rich in feldspar and detrital mica. Paleocurrent data, paleoslope data, sedimentary facies relationships, clast compositions, and detrital zircon ages from the upper Byrd units all suggest derivation and transport from igneous and

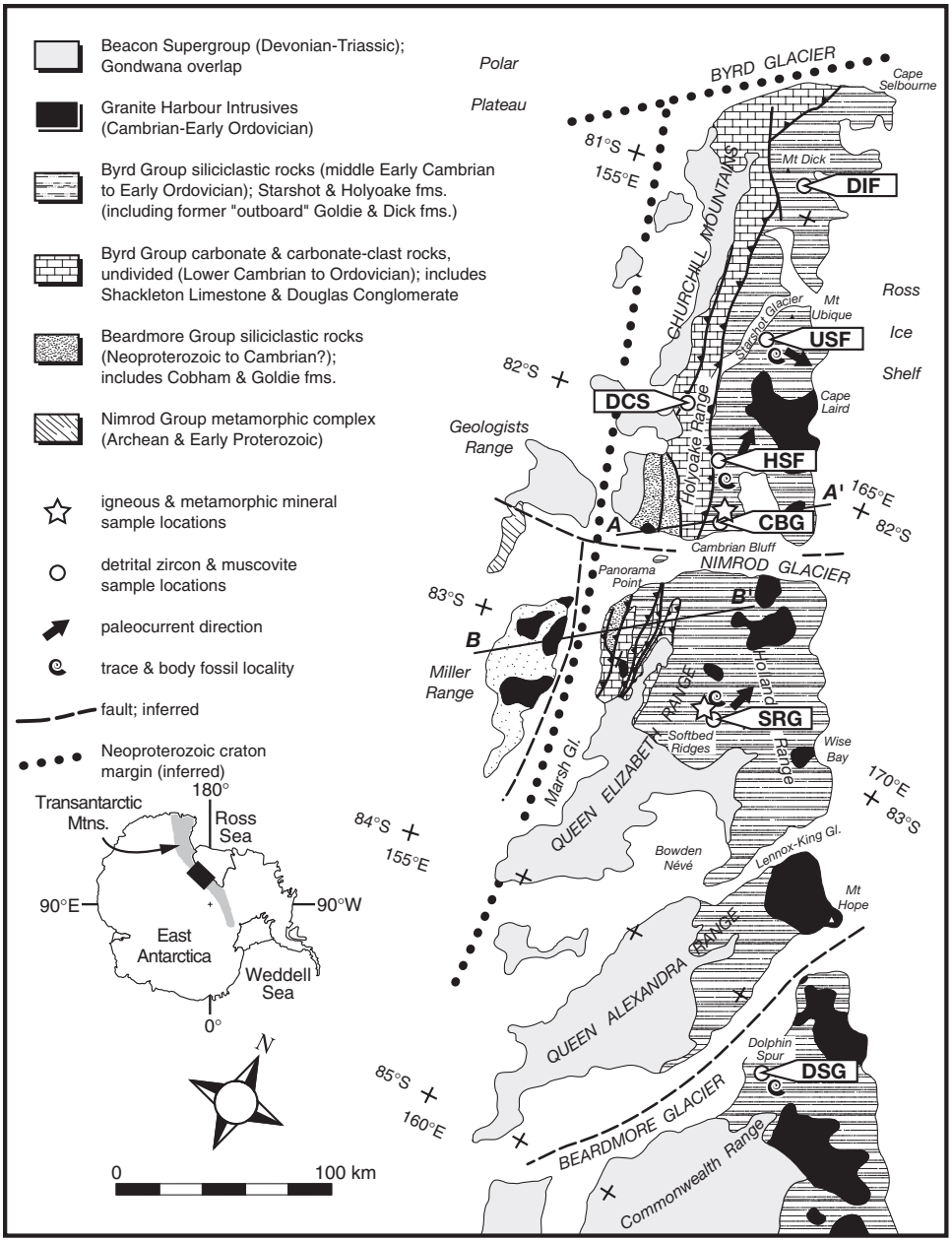


Figure 2. General geology of the central Transantarctic Mountains between Byrd and Beardmore glaciers, showing locations of dated samples. CBG—Starshot Fm., Cambrian Bluff; DCS—Douglas Conglomerate, Holyoake Range; DIF—Dick Fm., Cape Selbourne; DSG—Starshot Fm., Dolphin Spur; HSF—Starshot Fm., Holyoake Range; SRG—Starshot Fm., Softbed Ridges; USF—Starshot Fm., Mount Ubique. Sample information is given in Table 1. Stratigraphic assignment follows Myrow et al. (2002b) and Goodge et al. (2002), as shown in Figure 3. Schematic cross sections A–A′ and B–B′ shown in Figure 5.

metamorphic sources to the west in present-day coordinates (Myrow et al., 2002a, 2002b; Goodge et al., 2002). Syn- to post-tectonic igneous rocks of the Granite Harbour intrusive series, emplaced between ca. 540 and 480 Ma (Borg et al., 1990; Goodge et al., 1993b), intrude all units in the region.

The middle Early Cambrian to Ordovician upper Byrd Group, interpreted as forearc molasse deposits based on their sedimentary facies, detrital zircon characteristics, and position with respect to the magmatic arc (Goodge et al., 2002), therefore represents detritus derived from structurally thickened parts of the orogenic belt. These molasse units were derived in part from older metasedimentary rock units that were later thrust over them (Fig. 4). The molasse is a significant proportion of exposed rock in the present-day orogen, and it is itself deformed by open, upright structures and intruded by late-stage granitoids (Fig. 5).

Before the age and duration of denudation related to molasse deposition can be addressed using detrital mineral thermochronometry, it must be established that the minerals were eroded from the same source rock or from the same crustal level (Garver et al., 1999; Bernet et al., 2001). Evidence that zircon and muscovite in the upper Byrd Group molasse succession were derived from the same proximal sources includes the following: (a) the Starshot and Douglas formations are proximal deposits, based on their alluvial fan and marginal-marine sedimentary facies, immature compositions, degree of grain angularity, and preservation of pristine zircon crystals and coarse detrital muscovite

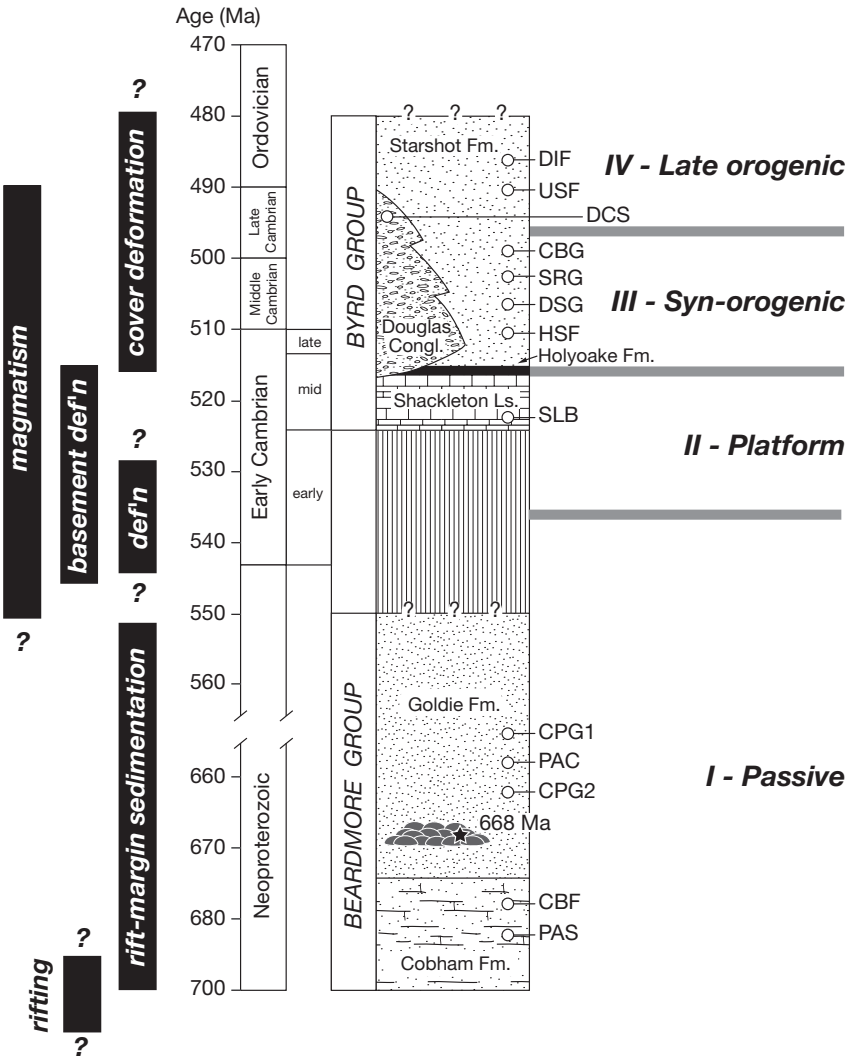


Figure 3. Stratigraphic relationships and detrital mineral samples in Neoproterozoic and lower Paleozoic sedimentary units of the central Transantarctic Mountains. Major time periods shown with Siberian biostratigraphic stages for reference. Revised stratigraphic relationships (Goodge et al., 2002; Myrow et al., 2002b) indicate passive-margin and platform deposition (stages I and II) through the middle Early Cambrian, when ramp carbonate of the Shackleton Limestone was abruptly overlapped by upward-coarsening siliciclastic deposits of the upper Byrd Group (stages III and IV; Holyoake, Starshot, and Douglas formations). Integration of biostratigraphic, chemostratigraphic, and geochronological data indicate that Shackleton carbonate deposition terminated ca. 515 Ma (Myrow et al., 2002b). Ages of geologic events in the central Ross Orogen summarized by black bars. Circles indicate units sampled for detrital mineral age determinations (see Table 1). DIF—Dick Formation, Cape Selbourne; USF—Starshot Formation, Mount Ubique; DCS—Douglas Conglomerate, Holyoake Range; CBG—Starshot Formation, Cambrian Bluff; SRG—Starshot Formation, Softbed Ridges; DSG—Starshot Formation, Dolphin Spur; HSF—Starshot Formation, Holyoake Range; SLB—Shackleton Limestone, Cotton Plateau; CPG1—Goldie Formation, Cotton Plateau; CPG2—Goldie Formation, Cotton Plateau; PAC—Goldie Formation (?) conglomerate, Princess Anne Glacier; CBF—Cobham Formation, Gargoyle Range; PAS—Goldie Formation (?) sandstone, Princess Anne Glacier.

grains, which all suggest short transport distance; (b) the presence of limestone clasts and crystalline calcite grains in some Starshot beds, in addition to igneous and quartzite clasts, suggesting that the Shackleton Limestone and local basement rocks were eroded; (c) the Starshot appears to have a chiefly intra-arc source, based on paleocurrents, sediment composition, zircon growth and radiogenic isotope characteristics, and trace minerals such as tourmaline (a distinctive accessory mineral in Ross-age igneous rocks of the region); and (d) the deposits immediately overlie autochthonous carbonate, suggesting that they are not far-traveled. If the detrital zircon and muscovite in the Starshot strata indeed share a common source, they can provide first-order constraints on the duration of denudation and sedimentation.

## ANALYTICAL METHODS

### $^{40}Ar/^{39}Ar$ Methods

Analytical procedures followed those described by McDougall and Feibel (1999). Muscovite and biotite mineral separates were prepared using standard crushing, desliming, heavy liquid, and paramagnetic techniques. Chips (0.5–1.0 mm) from two slate samples (CBGs1 and CBGs2) and ~30 detrital muscovite grains, from each of sandstone samples SRGm, CBGm, DSGm and USFm, were handpicked for $^{40}Ar/^{39}Ar$ analyses. The samples were ultrasonically cleaned in deionized water and acetone prior to submission for irradiation. All samples were wrapped in aluminum packets and placed in an aluminum irradiation canister together with interspersed aliquots of the flux monitor GA1550 biotite (age = 98.8 ± 0.5 Ma; Renne et al., 1998). Packets containing degassed potassium glass were placed at either end of the canister to monitor the $^{40}Ar$ production from potassium. The irradiation canister was irradiated for 504 hours in position X33 of the HIFAR reactor, Lucas Heights, Sydney. After irradiation, the samples were removed from their packaging and individual muscovite grains were loaded into 2-mm-diameter holes in a copper sample holder. After bake-out, single muscovite grains were fused using an argon-ion laser beam. Approximately 0.5 mg aliquots of biotite and ~1.0 mg of slate chips were wrapped in tinfoil, baked overnight, and step-heated in tantalum

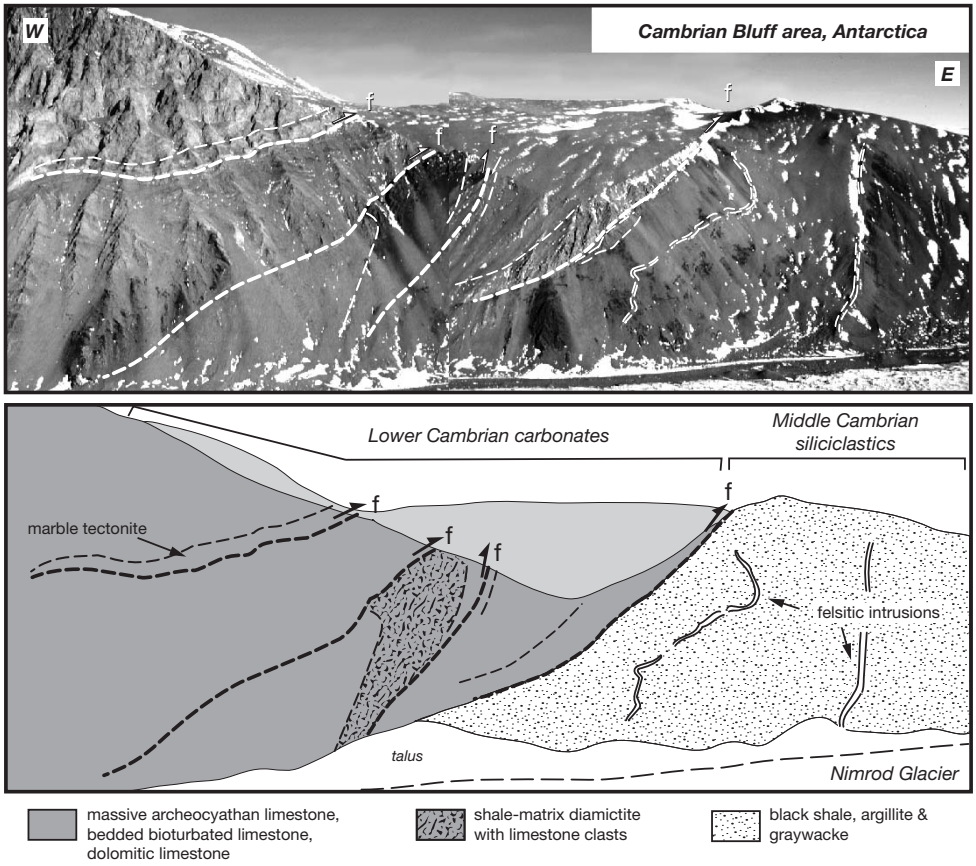


Figure 4. Outcrop photo mosaic of the eastern Cambrian Bluff area, southern Holyoake Range, showing older-over-younger structural relationship between Shackleton Limestone carbonate and Starshot Formation siliciclastic rocks. Massive outcrops to the west contain fault panels of different lithofacies in the Shackleton Limestone. Dark outcrops to the east are underlain by shale, argillite, sandstone, and diamictite of the Starshot Formation (formerly mapped as Goldie Formation; Laird et al., 1971). Line drawing shows interpretation of structures based on field, petrofabric, and age relationships. View to the north. Outcrop is ~800 m high. Samples CBG and 98-242 collected farther east of this outcrop area.

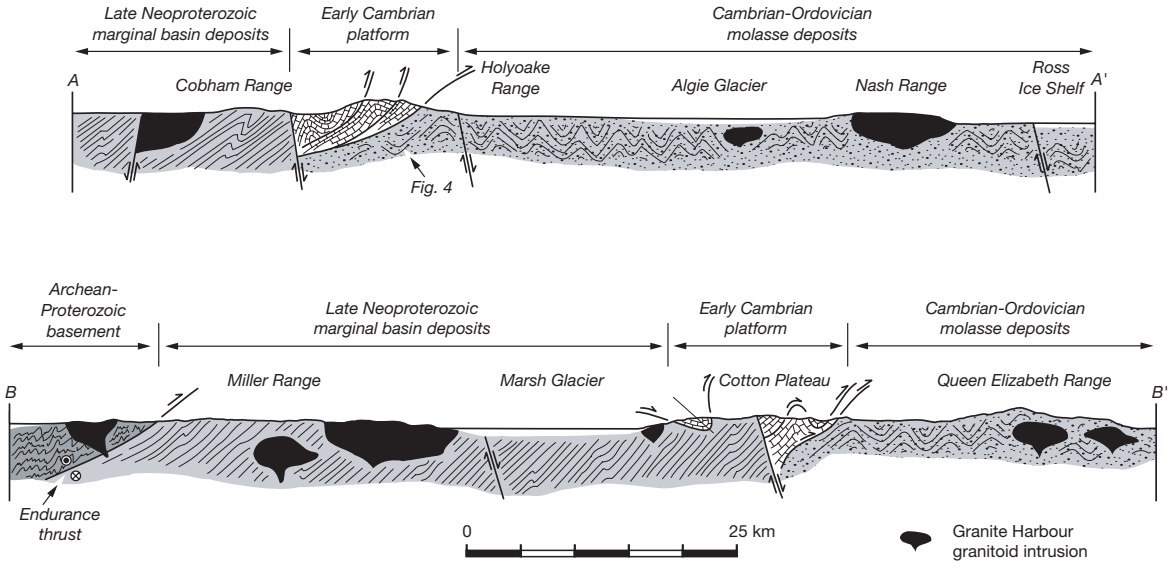


Figure 5. Schematic geologic cross sections of the Ross Orogen in the Nimrod Glacier area of the Transantarctic Mountains (see Fig. 2). Sections are approximately to scale with no vertical exaggeration. Molasse deposits of the Starshot Formation in the Holyoake, Nash, and Queen Elizabeth ranges are overridden by older (Early Cambrian) carbonate of the Shackleton Limestone, yet contain clasts of the carbonate as well as quartzitic material that was probably derived from crystalline basement and marginal-basin deposits presently exposed to the west.

resistance furnaces. $^{40}Ar/^{39}Ar$ analyses of muscovite and biotite samples were carried out at the Australian National University, whereas the two slate samples were analyzed at the University of Melbourne; all analyses were carried out on VG3600 mass spectrometers. Mass discrimination was monitored by analyses of standard air volumes. Correction factors for interfering reactions are as follows and apply to both labs: $(^{36}Ar/^{37}Ar)_{Ca} = 3.20 (\pm 0.02) \times 10^{-4}$; $(^{39}Ar/^{37}Ar)_{Ca} = 7.54 (\pm 0.5) \times 10^{-4}$ (Tetley et al., 1980); $(^{40}Ar/^{39}Ar)_{K} = 0.035 (\pm 0.005)$. K/Ca ratios were determined from the ANU laboratory hornblende standard 77-600 and were calculated as follows: $K/Ca = 1.90 \times {}^{39}Ar/^{37}Ar$. The reported data have been corrected for system backgrounds, mass discrimination, and radioactive decay. The $^{40}Ar^*/^{39}Ar$ ratios and ages have also been corrected for fluence gradients and atmospheric contamination. Errors associated with the age determinations are 1σ uncertainties and exclude errors in the J-value estimates. The error on the J-value is ± 0.3%, excluding the uncertainty in the age of GA1550. Decay constants are those of Steiger and Jäger (1977). McDougall and Harrison (1999) describe the $^{40}Ar/^{39}Ar$ dating technique in detail.

### U-Pb Methods

Detrital zircon procedures followed those described by Goodge et al. (2002). Heavy mineral concentrates of igneous zircon from the granitoids discussed here were prepared using standard crushing, desliming, heavy liquid, and paramagnetic techniques. Zircons were handpicked from the mineral concentrates, mounted in epoxy together with chips of the FC1 and SL13 reference zircons, sectioned approximately in half, and polished. Reflected and transmitted light photomicrographs and cathodoluminescence (CL) scanning electron microscope (SEM) images were prepared for all zircons. The CL images were used to decipher the internal structures of the sectioned grains and to target specific areas within the zircons for analysis. U-Pb analyses of zircons in the two igneous samples were made using sensitive high-resolution ion microprobe (SHRIMP) II at the National Institute for Polar Research, Tokyo. The analyses consisted of 6 scans through the mass range, and data were reduced in a manner similar to that described by Williams (1998, and references therein) using the SQUID Excel macro of Ludwig (2000). The Pb/U ratios are normalized relative to a value of 0.1859 for the $^{206}Pb/^{238}U$ ratio of the FC1 reference zircons, equivalent to an age of 1099 Ma (see Paces and Miller, 1993). Uncertainties given for individual analyses (ratios and ages) are at the 1σ level; however, the uncertainties in calculated weighted mean $^{206}Pb/^{238}U$ ages are reported as 95% confidence limits, including the uncertainty in the U-Pb calibration of the reference zircon. Tera-Wasserburg concordia plots, relative probability plots with stacked histograms, and weighted mean $^{206}Pb/^{238}U$ ages were prepared using ISOPLOT/EX (Ludwig, 1999).

## DETRITAL MINERAL AGES

Results of detrital zircon and muscovite analyses from Starshot and Douglas samples are summarized in Table 1. Here we discuss existing U-Pb age data for detrital zircons and present new $^{40}Ar/^{39}Ar$ ages for detrital muscovites.

### U-Pb Ages of Detrital Zircon

Detrital zircons were analyzed from 12 samples of sandstone from the central Ross Orogen that represent units deposited during the passive- to convergent-margin transition in Neoproterozoic to Ordovician time (Goodge et al., 2002; Goodge et al., 2004). This tectonic transition is well represented by the zircon age distributions, which show distinctive shifts in sedimentary provenance and depositional age. Late Neoproterozoic to Early Cambrian passive-margin and platform units of the Beardmore and lower Byrd groups, stages I and II in Figure 6, contain only Precambrian zircon. Although depositional ages are not precisely known for the passive-margin siliciclastic units, samples inferred

TABLE 1. SUMMARY OF DETRITAL GRAIN AGES, UPPER BYRD GROUP SILICICLASTICS, TRANSANTARCTIC MOUNTAINS, ANTARCTICA

| Area/stratigraphic unit | Sample No. | Youngest muscovite grains (Ma)† | Youngest zircon grains (Ma)§ | Maximum depositional age |
|---|---|---|---|---|
| Byrd-Nimrod-Beardmore glaciers area | | | | |
| Starshot Formation, Cape Selbourne* | DIF | | 501 ± 9 (5) | Late Cambrian |
| Starshot Formation, Mount Ubique | USF | 504 ± 3 (9) | 501 ± 5 (11) | Late Cambrian |
| Douglas Conglomerate, Holyoake Range | DCS | | 506 ± 6 (5) | late Middle Cambrian |
| Starshot Formation, Cambrian Bluff* | CBG | 510 ± 3 (4) | | Middle Cambrian |
| Starshot Formation, Holyoake Range | HSF | | 510 ± 12 (3) | Middle Cambrian |
| Starshot Formation, Softbed Ridges* | SRG | 518 ± 4 (6) | 531 ± 8 (4) | middle Early Cambrian |
| Starshot Formation, Dolphin Spur* | DSG | 516 ± 5 (6) | 547 ± 12 (4) | middle Early Cambrian |

* Units originally mapped as Goldie or Dick formation, now included in Starshot Formation (Myrow et al., 2002b).
† Weighted average of youngest discrete muscovite grain population; number of grains in parentheses.
§ Complete zircon data presented by Goodge et al. (2002) and Goodge et al. (2004). Ages represent weighted average of youngest discrete zircon grain population; number of grains in parentheses.

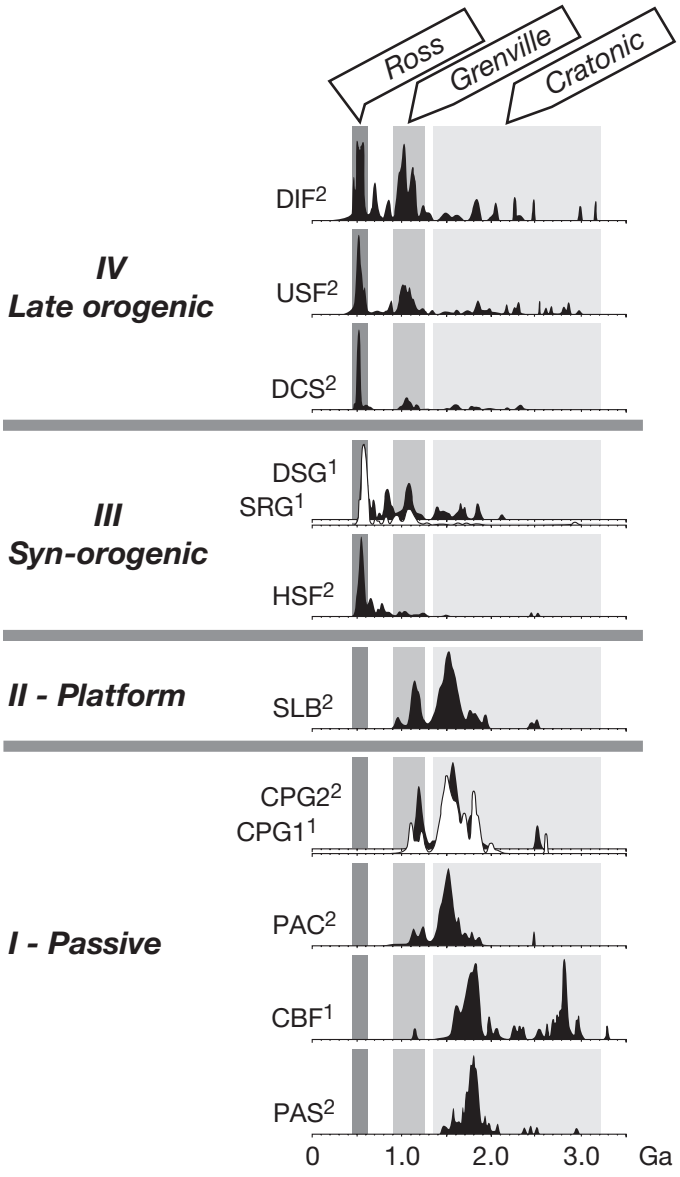


Figure 6. Summary of detrital zircon results from Beardmore and Byrd group sandstone (Goodge et al., 2002; Goodge et al., 2004), presented as relative probability histograms. Tectonic stages I–IV as in Figure 3, and detrital age results shown in order of relative depositional age based on biostratigraphic control and the youngest zircon grain populations. Provenance changes as follows: (I) passive-margin stage, characterized by Archean and Mesoproterozoic cratonic provenance; (II) platform stage, with mixed carbonate and siliciclastic deposition, the latter dominated by Mesoproterozoic and Grenville-age sources; (III) synorogenic stage, marked by near complete absence of cratonic and older orogenic (Grenville) signatures, and dominated by proximal, young material from the youthful Ross orogen; and (IV) late orogenic stage, showing the youngest detrital components with a Ross provenance, but also minor influx of older cratonic material. Samples as labeled in Figure 3. Original sources of age data as follows: 1—Goodge et al. (2002); 2—Goodge et al. (2004).

to come from stratigraphically lower units contain only Archean and Paleoproterozoic components (PAS and CBF), whereas they are succeeded by units dominated by Mesoproterozoic components, with increasing input of Grenville-orogen age (PAC, CPG, SLB). These age distributions are interpreted as the signature of a cratonic provenance, probably from the East Antarctic shield or adjacent cratonic areas (Goodge et al., 2002).

Siliciclastic deposits of the upper Byrd Group are regarded as syn- to late-tectonic in origin and show markedly different detrital zircon signatures compared to the older units (stages III and IV, Fig. 6). The age distributions of these younger sandstone deposits are simpler and dominated by a composite Ross age component ranging from ca. 600 to 500 Ma (HSF, SRG, DSG, DCS). The two youngest samples (USF, DIF) also contain significant amounts of first-cycle Precambrian material, including contributions from Grenville-age (ca. 995, 1035, 1080, 1130, and 1225 Ma) and older (ca. 3.1–3.0, 2.8, and 2.5 Ga) sources. Despite the dominant Ross signature, the Grenville-type and older cratonic ages indicate either that sediment deposition occurred close to exposures of cratonic basement or that it represents deep basement erosion. The morphology, growth zoning, and isotopic compositions of the young Ross-age zircons indicate mostly an igneous origin, which we interpret as the product of erosion from a continental-margin magmatic arc that developed during the main stage of the Ross Orogeny (Fig. 1C; Goodge et al., 2002). The general age distribution in the youngest samples is quite similar to that in Ordovician sandstone units of eastern Australia (Williams, 1998; Ireland et al., 1998), New Zealand (Ireland and Gibson, 1998), and South Africa (Armstrong et al., 1998) and may indicate the widespread distribution of sediments from a common source terrain along the Pacific margin of Gondwana during late Ross and Delamerian time (Williams et al., 2002).

In addition to source information, the detrital zircon ages from the upper Byrd sandstone units also confirm biostratigraphically constrained depositional ages. The youngest discrete detrital subpopulations in the Byrd Group units (ca. 550–500 Ma; Table 1) indicate maximum depositional ages between Early and Late Cambrian, consistent with the Botomian age for onset of siliciclastic deposition indicated by trilobites in the lower Starshot Formation. Radiometric dates on granitoid intrusions in the region also constrain deposition to be no younger than Early Ordovician. Detrital muscovite data, discussed below, help to further constrain the depositional ages for some of the samples.

### $^{40}Ar/^{39}Ar$ Ages of Detrital Muscovite

$^{40}Ar/^{39}Ar$ ages were measured on individual detrital muscovite grains from four sandstone samples of the upper Byrd Group. All were from the Starshot Formation (Table 1), although three (SRGm, CBGm, and DSGm) were collected from exposures originally mapped as Goldie Formation (Laird et al., 1971; Oliver, 1972). Detrital zircon age data (Goodge et al., 2002; Goodge et al., 2004) are available for samples SRGm, DSGm, and USFm. Detrital muscovite was distinguished from neoblastic muscovite

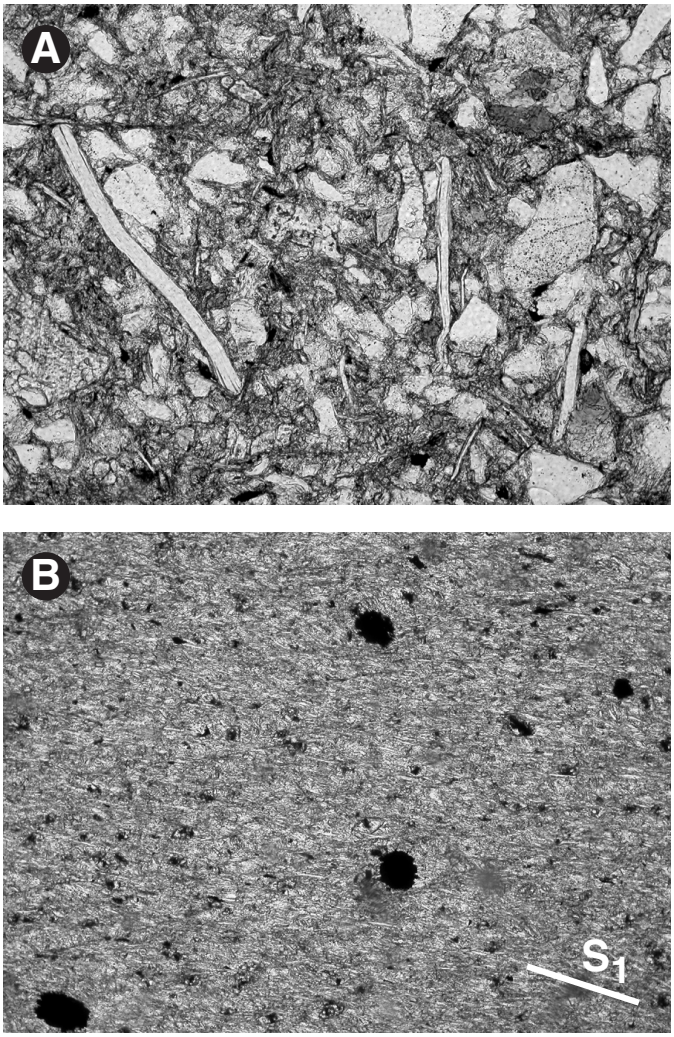


Figure 7. Thin section photomicrographs showing textural types of muscovite in Starshot Formation sandstones and shales. A: Immature feldspathic sandstone from Mount Ubique area (sample USFm) showing angular texture of framework grains, poor sorting, and elongate, bent detrital muscovite grains. Plane-polarized light (PPL); field of view ~1 mm. B: Slate from Cambrian Bluff area (sample CBGs) showing foliation ($S_1$) formed by fine-grained, neoblastic phyllosilicates, including colorless muscovite. Larger black clots are opaque minerals. PPL; field of view ~1 mm.

primarily by its size and shape. The grains are coarse (up to 1 mm) flakes similar in size to framework grains of quartz and feldspar, they have high aspect ratios (mostly 10:1 or greater), and they are typically bent or kinked where in contact with framework grains (Fig. 7A). Neoblastic metamorphic minerals, including muscovite, chlorite, and biotite, are finer grained and texturally distinctive (Fig. 7B). Single-grain $^{40}Ar/^{39}Ar$ fusion ages were obtained for 12–14 detrital muscovites from each sample using an Ar-ion laser. Analytical data are listed in Table 2 and the ages illustrated in Figure 8.

Sample SRGm was collected from the Lowery Glacier-Softbed Ridges area (Fig. 2). It is a fine to medium-grained (0.1–0.5 mm), feldspathic graywacke containing angular grains of quartz, plagioclase, muscovite, and lithic grains (slate and polycrystalline quartz), indicating a source composed of crystalline basement and low-grade metasedimentary rocks. Fourteen detrital muscovite grains yielded ages ranging from ca. 584 to 490 Ma (Fig. 8A), with two grains (1 and 11) much older than the rest (561 ± 3 Ma and 584 ± 12 Ma, respectively). The weighted mean age of the 12 younger grains is 507 ± 7 Ma, but there is considerable scatter beyond analytical error ($\chi^2 = 23.7$). This population is bimodal, with six grains yielding a weighted mean age of 497 ± 4 Ma ($\chi^2 = 3.1$) and the other six a weighted mean age of 518 ± 4 Ma ($\chi^2 = 2.5$). The mean age of the youngest grains in sample SRGm is indistinguishable from that of a nearby intrusion (see below), but the presence of some distinctly older grains suggests a maximum depositional age of 518 ± 4 Ma. If correct, this indicates that the sample has a middle Early Cambrian or younger depositional age, consistent with the less precise age limit of 531 ± 8 Ma provided by the youngest detrital zircons (Table 1).

Sample CBGm is a feldspathic arenite from the northeast end of Cambrian Bluff in the southern Holyoake Range (Fig. 2). It was collected immediately north of Nimrod Glacier and ~1 km west of the Errant Glacier confluence from prominent outcrops characterized by thick tabular beds of feldspathic wacke and shale. The sample is a medium-grained (0.5–1.0 mm) arenite containing angular to sub-angular quartz, plagioclase, K-feldspar, and muscovite, with minor biotite, tourmaline, sphene, and crystalline calcite. Lithic grains include biotite-rich quartzite, fine-grained quartzite, coarse polycrystalline quartz, myrmekitic quartz, quartz–muscovite schist, matrix-supported wacke, slate, and crenulated slate. The composition and texture of the grains indicate a proximal source that includes granite, metasedimentary rocks, limestone, and older siliciclastic rocks. Eleven muscovite grains yielded ages ranging from ~515 to 480 Ma (Fig. 8B), with a weighted mean age of 502 ± 8 Ma, but significant scatter ($\chi^2 = 7.8$). One other grain (2) with a small $^{39}Ar$ release, low radiogenic $^{40}Ar$ content, and a high Ca/K ratio yielded an imprecise age of 369 ± 143 Ma, likely due to alteration and/or contamination effects. This result is excluded from the population and is not shown on Figure 8. As in sample SRGm, the ages are bimodal, with seven grains yielding a weighted mean age of 486 ± 4 Ma (excluding grain 2) and four a weighted mean age of 510 ± 3 Ma. The former muscovite ages are younger than a crosscutting intrusion and probably reflect partial resetting of older detrital grains. If argon loss is minimal in the four oldest grains, then they indicate a Middle Cambrian or younger depositional age. This sample was not included in the detrital zircon study.

Sample DSGm was collected from an exposure of thin-bedded sandstone and shale near the crest of Dolphin Spur, ~12 km east of Beardmore Glacier and Mount Patrick (Fig. 2). These rocks show trough cross-beds, thin graded channel deposits, desiccation cracks, and small (~1 cm) burrows, indicating a shallow marine depositional setting. The sample is a fine-grained (≤0.5 mm) quartz graywacke containing quartz, plagioclase, muscovite, and lithics (polycrystalline quartz, slate, and muscovite schist), with minor Fe-Ti–oxide and tourmaline. Eleven

TABLE 2. $^{40}AR/^{39}AR$ LASER PROBE FUSION RESULTS FOR SINGLE MUSCOVITE GRAINS, STARSHOT FORMATION, UPPER BYRD GROUP, ANTARCTICA

| Grain no. | Analysis type | Mineral | Cum $^{39}Ar$ | $^{40}Ar/^{39}Ar$ | $^{37}Ar/^{39}Ar$ | $^{36}Ar/^{39}Ar$ | Vol. $^{39}Ar$ x$10^{-15}$mol | $^{40}Ar^*$ (%) | Ca/K | $^{40}Ar^*/^{39}Ar$ | Age (Ma) | ± 1 s.d. (Ma) |
|---|---|---|---|---|---|---|---|---|---|---|---|---|
| SRGm (98-210) J = 0.009439 ± 0.000028 | | | | | | | | | | | | |
| 1 | Fusion | Muscovite | 1.000 | 39.02 | 0.0158 | 0.0012 | 0.3685 | 99.0 | 0.0299 | 38.65 | 561.0 | 2.8 |
| 2 | Fusion | Muscovite | 1.000 | 33.88 | 0.0040 | 0.0017 | 0.2227 | 98.5 | 0.0077 | 33.37 | 493.9 | 6.1 |
| 3 | Fusion | Muscovite | 1.000 | 33.67 | 0.0001 | 0.0007 | 1.0640 | 99.3 | 0.0001 | 33.45 | 495.0 | 1.4 |
| 4 | Fusion | Muscovite | 1.000 | 35.64 | 0.0001 | 0.0008 | 0.6204 | 99.2 | 0.0002 | 35.36 | 519.6 | 3.2 |
| 5 | Fusion | Muscovite | 1.000 | 36.00 | 0.0938 | 0.0009 | 0.0508 | 99.2 | 0.1780 | 35.73 | 524.2 | 11.0 |
| 6 | Fusion | Muscovite | 1.000 | 34.33 | 0.0367 | 0.0004 | 0.1035 | 99.5 | 0.0696 | 34.17 | 504.2 | 7.6 |
| 7 | Fusion | Muscovite | 1.000 | 35.57 | 0.0048 | 0.0030 | 0.4088 | 97.4 | 0.0092 | 34.65 | 510.5 | 2.6 |
| 8 | Fusion | Muscovite | 1.000 | 35.24 | 0.0003 | 0.0003 | 1.4150 | 99.6 | 0.0006 | 35.10 | 516.2 | 2.1 |
| 9 | Fusion | Muscovite | 1.000 | 33.97 | 0.0039 | 0.0001 | 0.8374 | 99.8 | 0.0075 | 33.93 | 501.2 | 1.7 |
| 10 | Fusion | Muscovite | 1.000 | 35.65 | 0.0001 | 0.0006 | 1.7040 | 99.4 | 0.0001 | 35.44 | 520.6 | 1.6 |
| 11 | Fusion | Muscovite | 1.000 | 40.76 | 0.0055 | 0.0009 | 0.0671 | 99.3 | 0.0105 | 40.47 | 583.7 | 11.9 |
| 12 | Fusion | Muscovite | 1.000 | 33.64 | 0.0014 | 0.0017 | 0.5176 | 98.4 | 0.0027 | 33.10 | 490.5 | 2.6 |
| 13 | Fusion | Muscovite | 1.000 | 34.53 | 0.0010 | 0.0038 | 0.0827 | 96.7 | 0.0018 | 33.39 | 494.2 | 14.7 |
| 14 | Fusion | Muscovite | 1.000 | 35.28 | 0.0007 | 0.0004 | 0.8056 | 99.6 | 0.0014 | 35.12 | 516.5 | 2.2 |
| CBGm (98-233a) J = 0.009429 ± 0.000028 | | | | | | | | | | | | |
| 1 | Fusion | Muscovite | 1.000 | 33.70 | 0.0090 | 0.0025 | 0.2434 | 97.7 | 0.0171 | 32.93 | 487.9 | 5.4 |
| 2 | Fusion | Muscovite | 1.000 | 34.34 | 0.3619 | 0.0349 | 0.0090 | 70.0 | 0.6880 | 24.04 | 368.6 | 142.9 |
| 3 | Fusion | Muscovite | 1.000 | 33.88 | 0.0086 | 0.0047 | 0.2392 | 95.8 | 0.0164 | 32.44 | 481.4 | 7.1 |
| 4 | Fusion | Muscovite | 1.000 | 34.41 | 0.0003 | 0.0002 | 0.3179 | 99.7 | 0.0005 | 34.32 | 505.8 | 3.4 |
| 5 | Fusion | Muscovite | 1.000 | 33.79 | 0.0037 | 0.0025 | 0.4856 | 97.7 | 0.0071 | 33.01 | 488.9 | 3.6 |
| 6 | Fusion | Muscovite | 1.000 | 35.34 | 0.0192 | 0.0009 | 0.2586 | 99.1 | 0.0364 | 35.02 | 514.8 | 4.2 |
| 7 | Fusion | Muscovite | 1.000 | 35.86 | 0.0171 | 0.0081 | 0.0630 | 93.2 | 0.0325 | 33.42 | 494.2 | 13.8 |
| 8 | Fusion | Muscovite | 1.000 | 33.63 | 0.0257 | 0.0031 | 0.0878 | 97.2 | 0.0487 | 32.68 | 484.6 | 13.0 |
| 9 | Fusion | Muscovite | 1.000 | 34.80 | 0.0006 | 0.0004 | 0.6643 | 99.5 | 0.0012 | 34.65 | 510.0 | 2.1 |
| 10 | Fusion | Muscovite | 1.000 | 33.51 | 0.0118 | 0.0036 | 0.1900 | 96.8 | 0.0224 | 32.42 | 481.1 | 4.6 |
| 11 | Fusion | Muscovite | 1.000 | 34.68 | 0.0080 | 0.0005 | 0.2233 | 99.4 | 0.0152 | 34.49 | 507.9 | 5.9 |
| 12 | Fusion | Muscovite | 1.000 | 34.20 | 0.0125 | 0.0024 | 0.1488 | 97.8 | 0.0238 | 33.47 | 494.8 | 10.8 |
| DSGm (98-268F) J = 0.009525 ± 0.000028 | | | | | | | | | | | | |
| 1 | Fusion | Muscovite | 1.000 | 54.69 | 0.0356 | 0.0456 | 0.0023 | 75.3 | 0.0677 | 41.20 | 597.2 | 540.6 |
| 2 | Fusion | Muscovite | 1.000 | 35.15 | 0.0708 | 0.0012 | 0.6344 | 98.9 | 0.1350 | 34.78 | 516.2 | 1.7 |
| 3 | Fusion | Muscovite | 1.000 | 35.32 | 0.0003 | 0.0006 | 0.3199 | 99.4 | 0.0005 | 35.10 | 520.3 | 5.9 |
| 4 | Fusion | Muscovite | 1.000 | 37.81 | 0.0190 | 0.0070 | 0.1257 | 94.5 | 0.0362 | 35.72 | 528.4 | 7.3 |
| 5 | Fusion | Muscovite | 1.000 | 37.32 | 0.0185 | 0.0010 | 0.2181 | 99.1 | 0.0351 | 36.99 | 544.5 | 5.8 |
| 6 | Fusion | Muscovite | 1.000 | 36.34 | 0.0283 | 0.0016 | 0.4852 | 98.6 | 0.0537 | 35.82 | 529.6 | 3.0 |
| 7 | Fusion | Muscovite | 1.000 | 36.31 | 0.0059 | 0.0010 | 0.0630 | 99.1 | 0.0113 | 35.97 | 531.5 | 12.7 |
| 8 | Fusion | Muscovite | 1.000 | 36.29 | 0.0807 | 0.0043 | 0.0468 | 96.4 | 0.1530 | 34.98 | 518.9 | 22.7 |
| 9 | Fusion | Muscovite | 1.000 | 34.21 | 0.0080 | 0.0016 | 0.1737 | 98.5 | 0.0151 | 33.70 | 502.2 | 9.5 |
| 10 | Fusion | Muscovite | 1.000 | 34.39 | 0.0219 | 0.0025 | 0.1386 | 97.8 | 0.0416 | 33.62 | 501.2 | 8.1 |
| 11 | Fusion | Muscovite | 1.000 | 36.09 | 0.0078 | 0.0003 | 0.2000 | 99.7 | 0.0149 | 35.98 | 531.7 | 7.4 |
| 12 | Fusion | Muscovite | 1.000 | 35.86 | 0.0249 | 0.0028 | 0.3104 | 97.6 | 0.0474 | 35.02 | 519.3 | 5.2 |
| USFm (98-282A) J = 0.009554 ± 0.000028 | | | | | | | | | | | | |
| 1 | Fusion | Muscovite | 1.000 | 33.97 | 0.0100 | 0.0009 | 0.2575 | 99.1 | 0.0190 | 33.68 | 503.3 | 7.0 |
| 2 | Fusion | Muscovite | 1.000 | 32.80 | 0.0074 | 0.0003 | 0.0268 | 99.7 | 0.0140 | 32.70 | 490.5 | 14.3 |
| 3 | Fusion | Muscovite | 1.000 | 35.37 | 0.0019 | 0.0001 | 0.2963 | 99.8 | 0.0036 | 35.29 | 524.2 | 2.7 |
| 4 | Fusion | Muscovite | 1.000 | 34.38 | 0.0071 | 0.0012 | 0.5334 | 98.8 | 0.0134 | 33.98 | 507.2 | 2.6 |
| 5 | Fusion | Muscovite | 1.000 | 35.81 | 0.0116 | 0.0068 | 0.2021 | 94.3 | 0.0220 | 33.77 | 504.5 | 5.4 |
| 6 | Fusion | Muscovite | 1.000 | 33.81 | 0.0010 | 0.0010 | 1.0520 | 99.0 | 0.0018 | 33.47 | 500.5 | 1.9 |
| 7 | Fusion | Muscovite | 1.000 | 35.57 | 0.0048 | 0.0026 | 0.2108 | 97.7 | 0.0092 | 34.76 | 517.3 | 3.3 |
| 8 | Fusion | Muscovite | 1.000 | 33.66 | 0.0049 | 0.0001 | 0.2986 | 99.8 | 0.0093 | 33.57 | 501.9 | 6.9 |
| 9 | Fusion | Muscovite | 1.000 | 34.23 | 0.0144 | 0.0027 | 0.2279 | 97.6 | 0.0273 | 33.41 | 499.7 | 5.1 |
| 10 | Fusion | Muscovite | 1.000 | 34.58 | 0.0004 | 0.0010 | 0.2760 | 99.1 | 0.0008 | 34.27 | 510.9 | 3.8 |
| 11 | Fusion | Muscovite | 1.000 | 34.73 | 0.0000 | 0.0028 | 0.0289 | 97.5 | 0.0001 | 33.87 | 505.8 | 31.3 |
| 12 | Fusion | Muscovite | 1.000 | 33.27 | 0.0250 | 0.0031 | 0.2723 | 97.1 | 0.0476 | 32.31 | 485.4 | 3.6 |

*Note*: 1. Isotopic ratios are corrected for mass spectrometer backgrounds, mass discrimination and radioactive decay. 2. J-values are based on an age of 98.8 Ma for the GA1550 biotite monitor. 3. Errors are 1σ uncertainties and exclude the error in the J-value. 4. Correction factors: ($^{36}Ar/^{37}Ar$)Ca = 3.5E-4; ($^{39}Ar/^{37}Ar$)Ca = 7.86E-4; ($^{40}Ar/^{39}Ar$)K = 0.035; l40K = 5.543E-10.

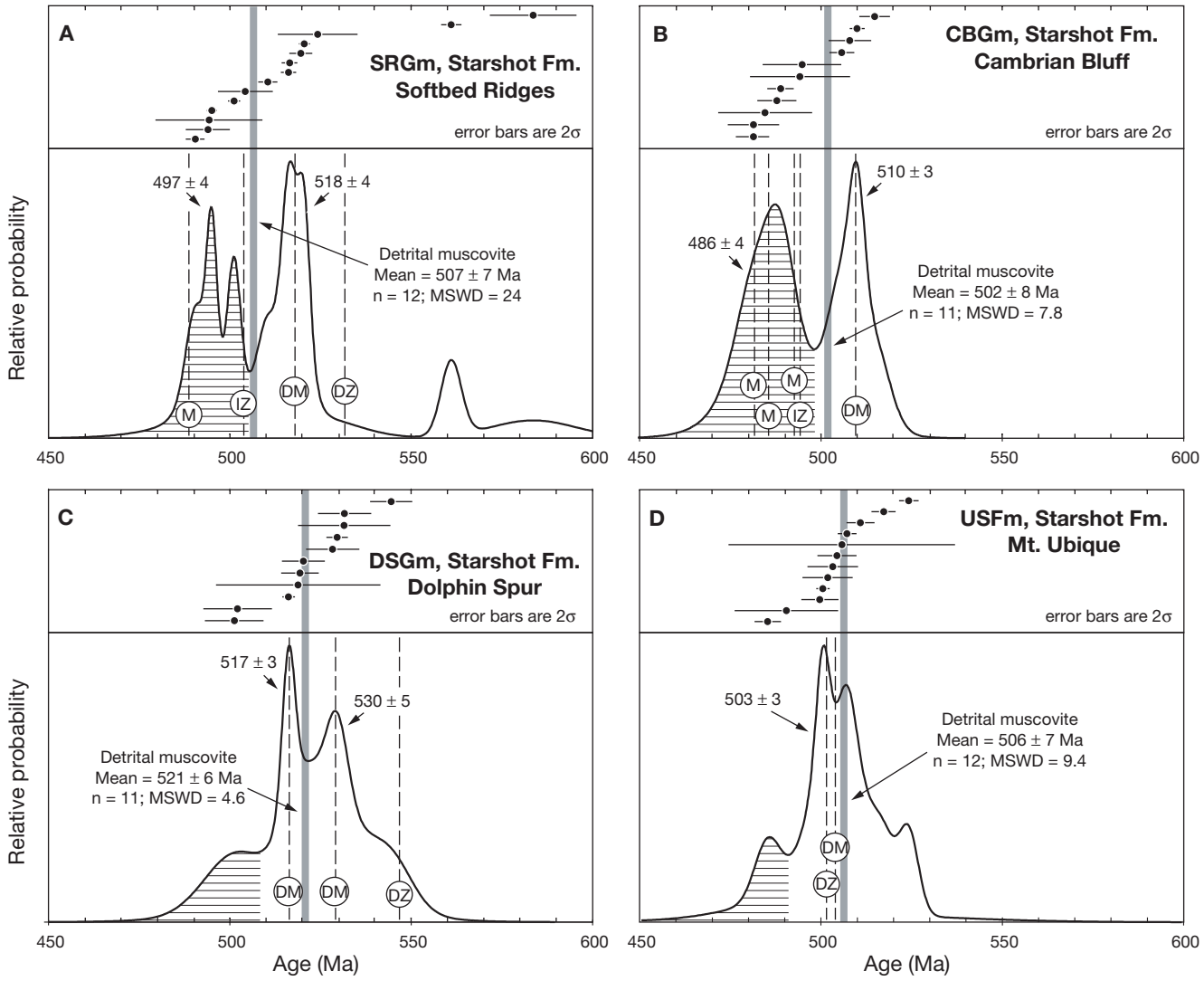


Figure 8. Single-grain $^{40}Ar/^{39}Ar$ laser probe fusion ages of detrital muscovites in samples of Starshot Formation sandstone. Upper panel for each sample shows individual grain analyses, with the 2σ error of each analysis (see Table 2). Lower panel shows relative probability distribution of all analyses in each sample, with ages of peaks indicated. Vertical gray bar indicates mean age of entire muscovite population, and dashed lines indicate ages of other events documented elsewhere in this paper. DM—detrital muscovite age mean; DZ—detrital zircon age mean; IZ—cross-cutting igneous zircon age; M—metamorphic age from slate or neoblastic biotite. Some analyses in samples CBGm and DSGm had large errors due to alteration or contamination and were excluded (see text).

muscovite grains yielded ages ranging from ~545 to 501 Ma (Fig. 8C), with a weighted mean age of 521 ± 6 Ma, but significant scatter ($\chi^2$ = 4.6). One other grain (1) produced little $^{39}Ar$, low radiogenic $^{40}Ar$, and yielded an imprecise age of 597 ± 541 Ma, attributed to alteration or contamination. It is excluded from the population and is not shown on Figure 8. As in the other samples, the mica ages are bimodal, but both peaks are substantially older than 500 Ma: five grains yielded a weighted mean age of 532 ± 8 and six grains an age of 516 ± 5 Ma. These results are compatible with other age constraints and there is no clear evidence of thermal overprinting. Assuming minimal argon loss, the younger group places the tightest constraint on the time of deposition, indicating a middle Early Cambrian or younger age. This is consistent with the older limit provided by detrital zircon (Table 1); excluding two grains that have probably lost Pb, the youngest detrital zircon subpopulation has an age of 547 ± 12 Ma (Goodge et al., 2002).

Sample USFm was collected from the Starshot Formation near Mount Ubique (Fig. 2). The formation here contains shale and tabular interbeds of sandstone with sedimentary structures that indicate shallow-water, wave-modified turbidity currents (Myrow et al., 2002a). Sample USFm, from an ~1 m thick massive sandstone bed, contains angular to subrounded quartz and feldspar (mostly plagioclase) with minor muscovite, biotite, tourmaline, crystalline calcite, and lithic grains (fine-grained quartz-muscovite schist). Thin, abraded muscovite flakes and

calcite grains suggest a proximal source. These, along with coarse monocrystalline quartz, plagioclase, and tourmaline, suggest a provenance that includes granite, limestone, and schistose metamorphic rocks. Twelve muscovite grains yielded ages ranging from 524 to 485 Ma (Fig. 8D), with a weighted mean age of 506 ± 7 Ma, but significant scatter ($\chi^2$ = 9.4). Excluding the youngest and two oldest grains, the remaining nine grains have a weighted mean age of 503 ± 3 Ma ($\chi^2$ = 1.2). Assuming minimal argon loss, these grains suggest a late Middle Cambrian or younger depositional age, consistent with the sample's higher stratigraphic position and the fact that it contains the youngest detrital zircon (501 ± 5 Ma; Table 1).

The similarity in detrital muscovite ages from these four Starshot samples suggests that they are from broadly coeval depositional units, despite minor sedimentary facies differences within the formation. Although there is evidence of argon loss for some detrital muscovites, the consistent presence of ca. 520 to 505 Ma muscovite in the different samples collectively indicates middle Early Cambrian or younger deposition ages (Table 1), in line with faunal ages from the basal part of the upper Byrd Group (ca. 515 Ma).

## POST-DEPOSITIONAL AGE CONSTRAINTS

The ages of crosscutting igneous rocks and metamorphic minerals in the Starshot Formation place upper limits on deposition age, thereby constraining the duration of sedimentation.

### Crosscutting Intrusions

Two crosscutting igneous intrusions were dated by SHRIMP zircon U-Pb to provide younger limits for the depositional age of the Starshot Formation. In the Softbed Ridges area (SRG in Fig. 2), the Starshot is intruded by medium- to coarse-grained hornblende-pyroxene quartz gabbro. The intrusive is small (<400 m across) with a sharp western contact where the gabbro has a diabasic texture and a gradational eastern contact with hornfelsic sandstone and calc-silicate layers containing veins and apophyses of diabase. The coarser interior phase contains xenoliths of metaarenite and argillite, and it shows no evidence of post-crystallization deformation. Zircon was analyzed from gabbro sample 98-207A, collected near the margin of the intrusion (Table 3). The sample contains coarse, concentrically zoned clinopyroxene

TABLE 3. SUMMARY OF SHRIMP U-PB ZIRCON RESULTS FOR QUARTZ GABBRO SAMPLE 98-207A, SOFTBED RIDGES, ANTARCTICA

| Grain spot | U (ppm) | Th (ppm) | Th/U | $^{206}Pb^*$ (ppm) | $^{204}Pb/^{206}Pb$ | $f_{206}$% | Total | | | | Radiogenic | | Age (Ma) | |
|---|---|---|---|---|---|---|---|---|---|---|---|---|---|---|
| | | | | | | | $^{238}U/^{206}Pb$ | ± | $^{207}Pb/^{206}Pb$ | ± | $^{206}Pb/^{238}U$ | ± | $^{206}Pb/^{238}U$ | ± |
| 1.1 | 1676 | 1630 | 0.97 | 115.6 | 0.000020 | 0.06 | 12.458 | 0.161 | 0.0576 | 0.0003 | 0.0802 | 0.0011 | 497.5 | 6.3 |
| 2.1 | 591 | 331 | 0.56 | 42.0 | 0.000094 | 0.14 | 12.107 | 0.144 | 0.0586 | 0.0006 | 0.0825 | 0.0010 | 510.9 | 5.9 |
| 3.1 | 596 | 327 | 0.55 | 41.6 | 0.000037 | 0.05 | 12.287 | 0.133 | 0.0577 | 0.0005 | 0.0813 | 0.0009 | 504.2 | 5.3 |
| 4.1 | 1689 | 1792 | 1.06 | 119.7 | 0.000045 | <0.01 | 12.116 | 0.121 | 0.0575 | 0.0003 | 0.0825 | 0.0008 | 511.2 | 5.0 |
| 5.1 | 1179 | 1258 | 1.07 | 81.4 | – | 0.13 | 12.449 | 0.141 | 0.0582 | 0.0004 | 0.0802 | 0.0009 | 497.4 | 5.5 |
| 6.1 | 1349 | 1459 | 1.08 | 95.2 | 0.000059 | 0.06 | 12.173 | 0.124 | 0.0580 | 0.0003 | 0.0821 | 0.0009 | 508.6 | 5.1 |
| 7.1 | 966 | 769 | 0.80 | 67.2 | 0.000050 | <0.01 | 12.349 | 0.124 | 0.0573 | 0.0004 | 0.0810 | 0.0008 | 502.0 | 4.9 |
| 8.1 | 1107 | 1051 | 0.95 | 78.1 | – | 0.03 | 12.174 | 0.148 | 0.0577 | 0.0004 | 0.0821 | 0.0010 | 508.7 | 6.1 |
| 9.1 | 812 | 721 | 0.89 | 56.3 | 0.000023 | 0.03 | 12.387 | 0.126 | 0.0575 | 0.0004 | 0.0807 | 0.0008 | 500.3 | 5.0 |
| 10.1 | 624 | 325 | 0.52 | 42.9 | – | 0.10 | 12.490 | 0.141 | 0.0579 | 0.0005 | 0.0800 | 0.0009 | 496.0 | 5.5 |
| 11.1 | 1164 | 1128 | 0.97 | 80.1 | – | 0.04 | 12.485 | 0.125 | 0.0575 | 0.0004 | 0.0801 | 0.0008 | 496.5 | 4.9 |
| 12.1 | 1483 | 1939 | 1.31 | 104.6 | – | <0.01 | 12.177 | 0.124 | 0.0572 | 0.0003 | 0.0822 | 0.0008 | 509.0 | 5.1 |
| 13.1 | 762 | 623 | 0.82 | 53.8 | – | 0.04 | 12.173 | 0.128 | 0.0578 | 0.0004 | 0.0821 | 0.0009 | 508.7 | 5.2 |
| 14.1 | 1757 | 1390 | 0.79 | 123.4 | 0.000023 | 0.08 | 12.233 | 0.129 | 0.0581 | 0.0003 | 0.0817 | 0.0009 | 506.1 | 5.2 |
| 15.1 | 1280 | 1058 | 0.83 | 89.0 | 0.000050 | 0.03 | 12.355 | 0.124 | 0.0575 | 0.0003 | 0.0809 | 0.0008 | 501.6 | 4.9 |
| 16.1 | 550 | 362 | 0.66 | 38.0 | 0.000001 | 0.09 | 12.454 | 0.129 | 0.0579 | 0.0005 | 0.0802 | 0.0008 | 497.5 | 5.0 |

*Note*: 1. Uncertainties given at the 1σ level; 2. Error in FC1 reference zircon calibration was 0.66% for the analytical session (not included in above errors but required when comparing data from different mounts); 3. $f_{206}$ % denotes the percentage of $^{206}Pb$ that is common Pb; 4. Correction for common Pb made using the measured $^{238}U/^{206}Pb$ and $^{207}Pb/^{206}Pb$ ratios following Tera and Wasserburg (1972) as outlined in Compston et al. (1992).

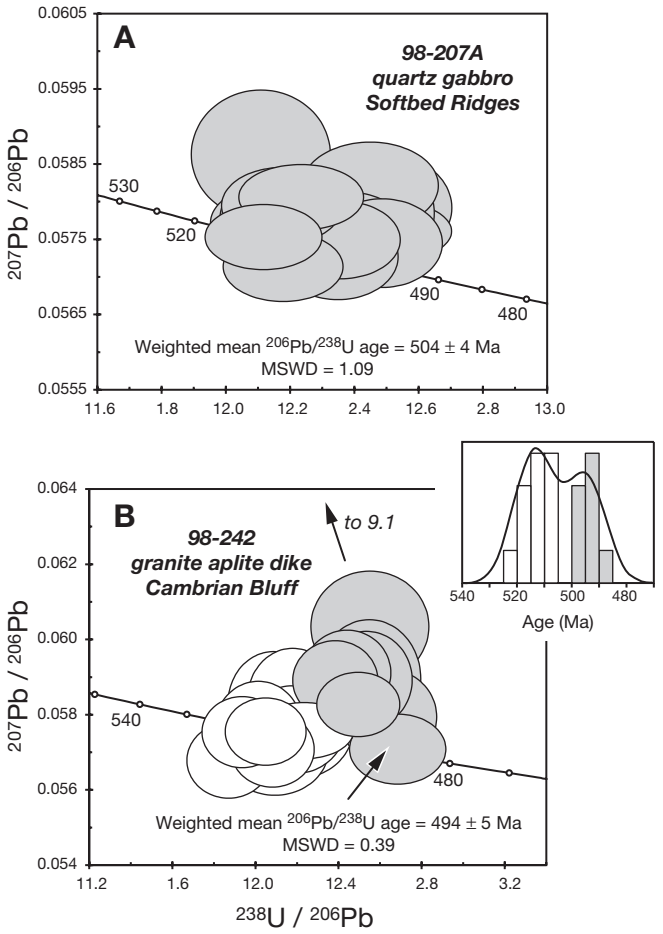


Figure 9. Tera-Wasserburg plots of U-Pb zircon ages obtained from igneous units crosscutting Starshot Formation sandstones. General location of samples correspond to SRG and CBG as shown in Figure 1, although intrusive rock units are too small to show at that scale. A: Quartz gabbro intruding sandstone at Softbed Ridges (sample 98-207A), with interpreted crystallization age of 504 ± 4 Ma from 16 zircon analyses (Table 3). B: Aplitic granite dike intruding sandstone and shale at east end of Cambrian Bluff (sample 98-242), showing two age subpopulations (see inset histogram). Separation of the ages into two populations indicates an early crystallization stage at 514 ± 5 Ma (weighted mean of 12 analyses indicated by white error ellipses) and a final crystallization age of 494 ± 5 Ma from the weighted mean of 8 zircon analyses comprising the younger population (gray error ellipses). Data presented in Table 4.

mantled by hornblende in a subophitic texture with interstitial quartz and plagioclase. Plagioclase and pyroxene are pervasively altered to calcite, biotite, chlorite, and epidote. The zircons are slender, prismatic grains with a simple, zoned magmatic internal structure as seen in CL imaging. They have moderate to high U and Th contents, yet all 16 analyses are concordant and have the same radiogenic $^{206}Pb/^{238}U$ within error (Fig. 9A). The weighted mean zircon age, including the error in the Pb/U calibration, is 503.5 ± 4.2 Ma. This is interpreted as the emplacement age of the gabbro. The gabbro crosscuts the sandstone sampled as SRG, constraining the deposition age to no younger than Middle Cambrian.

At the east end of Cambrian Bluff in the southern Holyoake Range (Fig. 2), folded carbonate of the Shackleton Limestone and black shale, argillite, and sandstone of the structurally underlying, but stratigraphically younger, Starshot Formation are intruded by leucocratic granite dikes up to 100 m wide (Fig. 4). The dikes have sharp contacts, fine grain size, light color, and massive texture. Sample 98-242 is from a muscovite-bearing aplitic granite dike that crosscuts black shale and sandstone sampled as CBG. Although internally massive, it becomes platy within ~2 m of its contacts, probably a result of flow while chilling. There is no textural evidence of significant subsolidus deformation, so the dike is interpreted to be post-tectonic. Zircons in the aplite are elongate euhedral crystals. CL images show that the grains have a mostly simple magmatic internal zonation; however, some of the central areas have discordant zoning that suggests an earlier phase of magmatic crystallization. Twenty zircon grains were analyzed for U-Th-Pb (Table 4, Fig. 9B). Their U and Th contents are normal for zircon from an unfractionated granitic rock. One grain (9.1) shows minor inheritance, but the other analyses are mostly concordant within error. They are not uniform in radiogenic $^{206}Pb/^{238}U$, but the scatter is low ($\chi^2 = 3.1$). The dispersion is not simply due to Pb loss from one or two grains, but to the fact that the compositions are bimodal, as shown by the histogram in Figure 9B. There is no correlation between apparent age and U, Th, or Th/U. The weighted mean $^{206}Pb/^{238}U$ ages of the two populations are 514 ± 5 (n = 12) and 494 ± 5 (n = 8) Ma, respectively, including uncertainty in the Pb/U calibration. Assuming no pervasive Pb loss, the younger population gives the best estimate of the age of emplacement. The older population possibly records an earlier stage of magma genesis. The age of the aplite therefore limits deposition of the Starshot Formation at Cambrian Bluff to no younger than Late Cambrian.

Combined with paleontologic evidence that siliciclastic deposition began at ca. 515 Ma (Myrow et al., 2002b), these igneous ages indicate that the Starshot Formation in the area of the Holyoake and Queen Elizabeth ranges is middle Early Cambrian to Late Cambrian in age. If the aplite sampled is cogenetic with other leucocratic dikes in the Cambrian Bluff outcrop that crosscut both the Shackleton and Starshot rocks, the two formations must also have been juxtaposed prior to ca. 495 Ma.

## Metamorphic Slate and Biotite

We determined $^{40}Ar/^{39}Ar$ ages for whole-rock slate and metamorphic biotite from samples of the Starshot Formation in order to determine the ages of post-depositional metamorphism and cooling. The $^{40}Ar/^{39}Ar$ method can be applied to low-temperature metamorphic rocks such as slates, although sometimes irradiation produces recoil loss and/or redistribution of $^{39}Ar$ in very fine-grained mineral components, resulting in discordant $^{40}Ar/^{39}Ar$ age spectra. We collected two slate samples from the eastern end of Cambrian Bluff (CBG in Fig. 2), where overturned beds of Starshot argillite, sandstone, and black shale show incipient formation of slaty cleavage, indicating lower

TABLE 4. SUMMARY OF SHRIMP U-PB ZIRCON RESULTS FOR GRANITE APLITE SAMPLE 98-242, CAMBRIAN BLUFF, ANTARCTICA

| Grain spot | U (ppm) | Th (ppm) | Th/U | $^{206}Pb^*$ (ppm) | $^{204}Pb/^{206}Pb$ | $f_{206}$% | Total | | | | Radiogenic | | Age (Ma) | |
|---|---|---|---|---|---|---|---|---|---|---|---|---|---|---|
| | | | | | | | $^{238}U/^{206}Pb$ | ± | $^{207}Pb/^{206}Pb$ | ± | $^{206}Pb/^{238}U$ | ± | $^{206}Pb/^{238}U$ | ± |
| 1.1 | 183 | 45 | 0.25 | 12.5 | – | 0.41 | 12.548 | 0.188 | 0.0603 | 0.0010 | 0.0794 | 0.0012 | 492.4 | 7.2 |
| 2.1 | 576 | 152 | 0.26 | 39.2 | – | 0.12 | 12.635 | 0.156 | 0.0580 | 0.0008 | 0.0791 | 0.0010 | 490.5 | 5.9 |
| 3.1 | 264 | 54 | 0.20 | 18.6 | 0.000010 | 0.03 | 12.206 | 0.173 | 0.0577 | 0.0009 | 0.0819 | 0.0012 | 507.5 | 7.0 |
| 4.1 | 580 | 242 | 0.42 | 39.3 | – | 0.02 | 12.682 | 0.153 | 0.0571 | 0.0006 | 0.0788 | 0.0010 | 489.1 | 5.8 |
| 5.1 | 168 | 41 | 0.24 | 11.5 | 0.000277 | 0.24 | 12.544 | 0.164 | 0.0590 | 0.0010 | 0.0795 | 0.0011 | 493.3 | 6.3 |
| 6.1 | 244 | 67 | 0.28 | 16.7 | 0.000187 | 0.23 | 12.530 | 0.146 | 0.0589 | 0.0008 | 0.0796 | 0.0009 | 493.9 | 5.6 |
| 7.1 | 275 | 86 | 0.31 | 19.4 | – | 0.02 | 12.176 | 0.163 | 0.0576 | 0.0008 | 0.0821 | 0.0011 | 508.7 | 6.7 |
| 8.1 | 234 | 49 | 0.21 | 16.6 | 0.000183 | <0.01 | 12.088 | 0.172 | 0.0571 | 0.0008 | 0.0828 | 0.0012 | 512.6 | 7.1 |
| 9.1 | 369 | 127 | 0.34 | 27.4 | 0.000988 | 3.33 | 11.569 | 0.126 | 0.0848 | 0.0009 | 0.0836 | 0.0010 | 517.3 | 5.9 |
| 10.1 | 195 | 53 | 0.27 | 13.9 | 0.000253 | 0.00 | 12.007 | 0.141 | 0.0576 | 0.0009 | 0.0833 | 0.0010 | 515.7 | 6.0 |
| 11.1 | 173 | 43 | 0.25 | 12.3 | 0.000232 | 0.10 | 12.080 | 0.144 | 0.0583 | 0.0009 | 0.0827 | 0.0010 | 512.2 | 6.0 |
| 12.1 | 482 | 141 | 0.29 | 33.2 | – | 0.15 | 12.491 | 0.131 | 0.0583 | 0.0006 | 0.0799 | 0.0009 | 495.8 | 5.1 |
| 13.1 | 326 | 83 | 0.25 | 23.2 | 0.000086 | <0.01 | 12.077 | 0.132 | 0.0571 | 0.0007 | 0.0828 | 0.0009 | 513.1 | 5.5 |
| 14.1 | 330 | 53 | 0.16 | 22.9 | – | 0.21 | 12.380 | 0.135 | 0.0589 | 0.0007 | 0.0806 | 0.0009 | 499.7 | 5.4 |
| 15.1 | 356 | 116 | 0.33 | 25.8 | 0.000014 | <0.01 | 11.865 | 0.132 | 0.0568 | 0.0007 | 0.0844 | 0.0010 | 522.2 | 5.7 |
| 16.1 | 368 | 136 | 0.37 | 26.5 | 0.000038 | <0.01 | 11.931 | 0.128 | 0.0576 | 0.0006 | 0.0838 | 0.0009 | 519.0 | 5.5 |
| 17.1 | 174 | 45 | 0.26 | 12.3 | – | 0.12 | 12.174 | 0.144 | 0.0584 | 0.0009 | 0.0820 | 0.0010 | 508.3 | 5.9 |
| 18.1 | 527 | 190 | 0.36 | 37.0 | 0.000024 | 0.03 | 12.229 | 0.159 | 0.0576 | 0.0005 | 0.0817 | 0.0011 | 506.5 | 6.4 |
| 19.1 | 250 | 40 | 0.16 | 17.2 | – | 0.24 | 12.438 | 0.139 | 0.0591 | 0.0007 | 0.0802 | 0.0009 | 497.3 | 5.4 |
| 20.1 | 361 | 100 | 0.28 | 25.7 | 0.000084 | <0.01 | 12.043 | 0.128 | 0.0576 | 0.0006 | 0.0830 | 0.0009 | 514.2 | 5.4 |

*Note*: 1. Uncertainties given at the 1σ level; 2. Error in FC1 reference zircon calibration was 0.66% for the analytical session (not included in above errors but required when comparing data from different mounts); 3. $f_{206}$ % denotes the percentage of $^{206}Pb$ that is common Pb; 4. Correction for common Pb made using the measured $^{238}U/^{206}Pb$ and $^{207}Pb/^{206}Pb$ ratios following Tera and Wasserburg (1972) as outlined in Compston et al. (1992).

greenschist-facies metamorphism (chlorite- to biotite-zone). Sandstone beds here show convolute bedding, load casts, and ripple-drift cross-beds, as well as graded bedding. Some of the coarse sandstone beds contain quartz granules, clasts of fine-grained quartzite, and black shale clasts. Although we refer to some strata and clasts in sandstone as shale, they have macroscopic parting surfaces indicating incipient slaty or phyllitic mineral growth. Sample CBGs1 consists of small, very fine-grained slate clasts (<3 cm) collected from a sandstone bed at the base of the exposure next to Nimrod Glacier. The clasts are interpreted as forming an intraformational conglomerate because they are concentrated within certain beds and oriented generally parallel to the principal composition plane. The chips contain neoblastic muscovite, biotite, and less common chlorite; the phyllosilicates are oriented parallel to compositional layering and elongation of the chips, but small ellipsoidal opaque minerals delineate a grain-shape alignment at a small angle to that foliation, suggesting a component of shear during recrystallization. The results of conventional step-heating analysis of the chips are listed in Table 5; two sets of data were collected, one at the Australian National University and the other at the University of Melbourne. Results of the second set of analyses are shown in Figure 10A. The step-heating data define a discordant, sigmoidal to saddle-shaped age spectrum common in fine-grained recrystallized materials that contain multiple mica components and have undergone minor recoil redistribution and/or loss of $^{39}Ar$ (e.g., Fergusson and Phillips, 2001). The younger ages obtained at low temperature are probably due to argon loss, and older ages from the high-temperature steps probably come from an older detrital component. The release spectrum includes a five-step intermediate age "plateau" (representing 43% of the $^{39}Ar$ released) of 492 ± 4 Ma. If the sample has undergone only recoil redistribution of $^{39}Ar$, then the age spectrum indicates an age of ca. 490 Ma for new metamorphic white mica crystallization in the slate. If the sample has suffered some recoil loss of $^{39}Ar$, then the age of metamorphism might be slightly younger (480 Ma). These ages post-date the older group of detrital muscovites from the Starshot sandstone sample at the same locality (CBGm, 510 ± 3 Ma, Fig. 8B), but they are indistinguishable from the ages of the younger muscovite grains (486 ± 4 Ma) and the crosscutting aplite dike (494 ±

TABLE 5. $^{40}AR/^{39}AR$ STEP-HEATING RESULTS FOR WHOLE-ROCK SLATE SAMPLES, STARSHOT FORMATION, UPPER BYRD GROUP, ANTARCTICA

| Temp (°C) | Cum $^{39}Ar$ | $^{40}Ar/^{39}Ar$ | $^{37}Ar/^{39}Ar$ | $^{36}Ar/^{39}Ar$ | Vol. $^{39}Ar$ $\times10^{-15}$mol | %Rad. $^{40}Ar$ | Ca/K | $^{40}Ar^*/^{39}Ar$ | Age (Ma) | ± 1s.d. (Ma) |
|---|---|---|---|---|---|---|---|---|---|---|
| CBGs1 (98-233C) WR Slate (ANU) Mass = 0.87 mg; J-value = 0.009429 ± 0.000028 | | | | | | | | | | |
| 550 | 0.0074 | 16.02 | 0.0913 | 0.0204 | 0.387 | 62.1 | 0.1730 | 9.95 | 161.8 | 5.1 |
| 600 | 0.0129 | 18.87 | 0.0327 | 0.0152 | 0.290 | 76.0 | 0.0621 | 14.35 | 228.9 | 6.5 |
| 650 | 0.0252 | 15.25 | 0.0154 | 0.0060 | 0.645 | 88.1 | 0.0293 | 13.43 | 215.1 | 2.9 |
| 700 | 0.0514 | 16.55 | 0.0131 | 0.0030 | 1.375 | 94.4 | 0.0248 | 15.62 | 247.9 | 1.3 |
| 740 | 0.0873 | 27.22 | 0.0070 | 0.0026 | 1.883 | 97.0 | 0.0132 | 26.41 | 401.2 | 1.3 |
| 760 | 0.1229 | 33.07 | 0.0044 | 0.0030 | 1.869 | 97.2 | 0.0084 | 32.14 | 477.6 | 1.4 |
| 780 | 0.1684 | 34.29 | 0.0020 | 0.0022 | 2.384 | 98.0 | 0.0038 | 33.60 | 496.5 | 1.4 |
| 800 | 0.2266 | 34.35 | 0.0040 | 0.0016 | 3.054 | 98.5 | 0.0076 | 33.85 | 499.7 | 1.4 |
| 820 | 0.2949 | 34.10 | 0.0047 | 0.0017 | 3.581 | 98.4 | 0.0089 | 33.56 | 496.0 | 1.1 |
| 840 | 0.3732 | 33.97 | 0.0033 | 0.0012 | 4.063 | 98.9 | 0.0063 | 33.59 | 496.4 | 1.1 |
| 860 | 0.4642 | 33.84 | 0.0012 | 0.0012 | 4.820 | 98.8 | 0.0023 | 33.44 | 494.5 | 1.2 |
| 880 | 0.5704 | 33.69 | 0.0005 | 0.0009 | 5.568 | 99.1 | 0.0010 | 33.39 | 493.8 | 1.1 |
| 900 | 0.6884 | 33.32 | 0.0019 | 0.0009 | 6.191 | 99.1 | 0.0037 | 33.01 | 488.9 | 1.0 |
| 925 | 0.8252 | 33.23 | 0.0010 | 0.0008 | 7.177 | 99.2 | 0.0020 | 32.96 | 488.2 | 1.1 |
| 1100 | 0.9245 | 34.52 | 0.0134 | 0.0018 | 5.211 | 98.4 | 0.0255 | 33.96 | 501.1 | 1.1 |
| 1200 | 0.9916 | 37.17 | 0.0717 | 0.0042 | 3.519 | 96.6 | 0.1360 | 35.89 | 525.9 | 1.6 |
| 1300 | 0.9972 | 53.02 | 0.6065 | 0.0724 | 0.294 | 59.7 | 1.1500 | 31.66 | 471.3 | 9.1 |
| 1450 | 1.0000 | 211.7 | 1.3583 | 0.6960 | 0.146 | 2.9 | 2.5800 | 6.19 | 102.3 | 43.7 |
| Total | | 33.49 | 0.0165 | 0.0042 | 52.46 | | | 32.21 | 478.4 | 1.4 |
| CBGs1 (98-233C) WR Slate (UM) Mass = 0.71 mg; J-value = 0.009429 ± 0.000028 | | | | | | | | | | |
| 600 | 0.1486 | 31.85 | 0.0516 | 0.0041 | 2.987 | 96.1 | 0.0980 | 30.60 | 457.3 | 1.7 |
| 650 | 0.2352 | 35.43 | 0.0407 | 0.0030 | 3.785 | 97.4 | 0.0773 | 34.51 | 508.2 | 4.0 |
| 700 | 0.3376 | 33.94 | 0.0403 | 0.0015 | 3.824 | 98.6 | 0.0766 | 33.47 | 494.8 | 6.5 |
| 750 | 0.4380 | 33.11 | 0.0351 | 0.0009 | 4.388 | 99.1 | 0.0667 | 32.82 | 486.4 | 2.8 |
| 775 | 0.5118 | 33.87 | 0.0478 | 0.0016 | 3.227 | 98.5 | 0.0907 | 33.39 | 493.8 | 2.9 |
| 800 | 0.5926 | 34.00 | 0.0437 | 0.0015 | 3.529 | 98.6 | 0.0830 | 33.52 | 495.4 | 2.4 |
| 825 | 0.6632 | 33.68 | 0.0499 | 0.0017 | 3.088 | 98.4 | 0.0948 | 33.16 | 490.9 | 2.5 |
| 850 | 0.7539 | 34.04 | 0.0389 | 0.0009 | 3.963 | 99.1 | 0.0739 | 33.73 | 498.2 | 1.8 |
| 875 | 0.8242 | 34.34 | 0.0502 | 0.0010 | 3.072 | 99.0 | 0.0953 | 34.02 | 501.9 | 2.8 |
| 900 | 0.8651 | 35.41 | 0.0862 | 0.0022 | 1.787 | 98.1 | 0.1640 | 34.74 | 511.2 | 2.7 |
| 925 | 0.8905 | 35.77 | 0.1415 | 0.0033 | 1.111 | 97.2 | 0.2690 | 34.79 | 511.8 | 2.7 |
| 950 | 0.9125 | 36.05 | 0.1631 | 0.0031 | 0.964 | 97.4 | 0.3100 | 35.12 | 516.1 | 3.0 |
| 1000 | 0.9431 | 36.07 | 0.1178 | 0.0016 | 1.335 | 98.6 | 0.2240 | 35.58 | 522.0 | 2.8 |
| 1050 | 0.9652 | 36.51 | 0.1626 | 0.0024 | 0.967 | 98.0 | 0.3090 | 35.79 | 524.5 | 3.0 |
| 1100 | 0.9914 | 37.71 | 0.1496 | 0.0051 | 1.051 | 96.0 | 0.2840 | 36.19 | 529.7 | 2.7 |
| 1300 | 0.9926 | 157.4 | 3.0878 | 0.3184 | 0.005 | 40.4 | 5.8800 | 63.67 | 848.4 | 70.5 |
| 1450 | 1.0000 | 310.1 | 0.4865 | 0.8567 | 0.323 | 18.3 | 0.9240 | 56.90 | 774.9 | 80.8 |
| Total | | 36.679 | 0.0669 | 0.0094 | 39.45 | | | 33.89 | 500.3 | 3.7 |
| CBGs2 (98-238) WR Slate (UM) Mass = 0.79 mg; J-value = 0.009429 ± 0.000028 | | | | | | | | | | |
| 600 | 0.1332 | 31.07 | 0.0350 | 0.0013 | 4.068 | 98.7 | 0.0665 | 30.65 | 458.0 | 1.7 |
| 650 | 0.2612 | 33.60 | 0.0364 | 0.0011 | 3.911 | 98.9 | 0.0692 | 33.24 | 491.9 | 2.1 |
| 700 | 0.3545 | 32.97 | 0.0499 | 0.0006 | 2.851 | 99.3 | 0.0949 | 32.76 | 485.6 | 1.5 |
| 750 | 0.4962 | 32.96 | 0.0329 | 0.0011 | 4.329 | 99.0 | 0.0625 | 32.62 | 483.8 | 1.4 |
| 775 | 0.6057 | 33.00 | 0.0425 | 0.0002 | 3.349 | 99.7 | 0.0808 | 32.90 | 487.5 | 1.5 |
| 800 | 0.6968 | 32.76 | 0.0512 | 0.0008 | 2.782 | 99.2 | 0.0973 | 32.50 | 482.3 | 2.0 |
| 825 | 0.7770 | 32.87 | 0.0267 | 0.0009 | 5.327 | 99.1 | 0.0508 | 32.58 | 483.2 | 2.0 |
| 850 | 0.8469 | 32.79 | 0.0307 | 0.0012 | 4.645 | 98.8 | 0.0582 | 32.40 | 481.0 | 1.4 |
| 875 | 0.9011 | 33.21 | 0.0396 | 0.0012 | 3.595 | 98.9 | 0.0752 | 32.83 | 486.5 | 2.2 |
| 900 | 0.9380 | 33.66 | 0.0581 | 0.0009 | 2.452 | 99.1 | 0.1100 | 33.37 | 493.5 | 1.7 |
| 925 | 0.9635 | 34.63 | 0.0840 | 0.0024 | 1.695 | 97.9 | 0.1600 | 33.89 | 500.3 | 2.6 |
| 950 | 0.9744 | 36.37 | 0.1972 | 0.0038 | 0.722 | 96.8 | 0.3750 | 35.22 | 517.3 | 2.8 |
| 1000 | 0.9855 | 37.59 | 0.1954 | 0.0021 | 0.743 | 98.3 | 0.3710 | 36.97 | 539.5 | 3.3 |
| 1050 | 0.9981 | 38.94 | 0.1735 | 0.0016 | 0.837 | 98.7 | 0.3300 | 38.45 | 558.0 | 3.9 |
| 1100 | 0.9986 | 49.01 | 0.4407 | 0.0015 | 0.033 | 99.1 | 0.8380 | 48.57 | 680.3 | 11.1 |
| 1200 | 0.9998 | 56.33 | 0.1903 | 0.0002 | 0.076 | 99.9 | 0.3620 | 56.25 | 767.7 | 10.7 |
| 1300 | 1.0000 | 316.5 | 1.0035 | 0.0011 | 0.014 | 99.9 | 1.9100 | 316.5 | 2493.8 | 50.5 |
| Total | | 33.33 | 0.0350 | 0.0011 | 41.43 | | | 32.99 | 488.6 | 1.9 |

*Note*: 1. Errors are 1σ uncertainties and exclude uncertainties in the J-value. 2. Data are corrected for mass spectrometer backgrounds, discrimination and radioactive decay. 3. Interference corrections: $(^{36}Ar/^{37}Ar)_{Ca}$ = 3.2E-4; $(^{39}Ar/^{37}Ar)_{Ca}$ = 7.86E-4; $(^{40}Ar/^{39}Ar)_{K}$ = 3.50E-2. 4. J-value is based on an age of 98.8 Ma for GA-1550 biotite. 5. Samples analyzed at Australian National University (ANU) and University of Melbourne (UM).

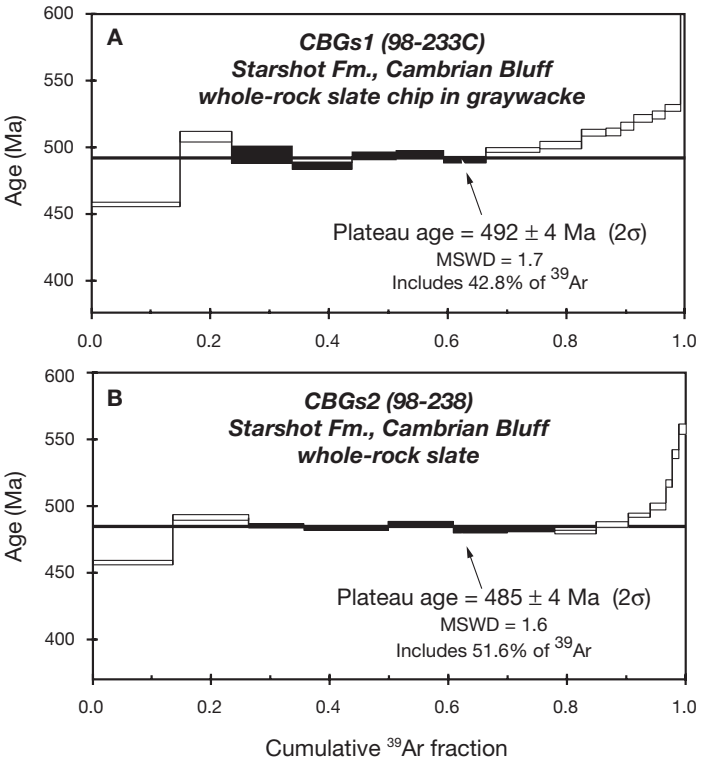


Figure 10. Ar release spectra from step-heating analyses of whole-rock slate samples obtained in the Starshot Formation at the east end of Cambrian Bluff (Fig. 2). Both samples show sigmoidal, saddle-shaped spectra with some inherited older age components, which reflect the competing influences of argon loss, argon recoil loss/redistribution, and incomplete resetting of detrital components. Plateau ages were assigned for the steps indicated in black, although the age of metamorphism may be slightly older (see text). A: Sample CBGs1 (98-233C), consisting of slate chips separated from a poorly-sorted graywacke, yielded a plateau age of 492 ± 4 Ma (2σ error). B: Sample CGBs2 (98-238), a coherent laminated slate, yielded a plateau age of 485 ± 4 Ma (2σ error).

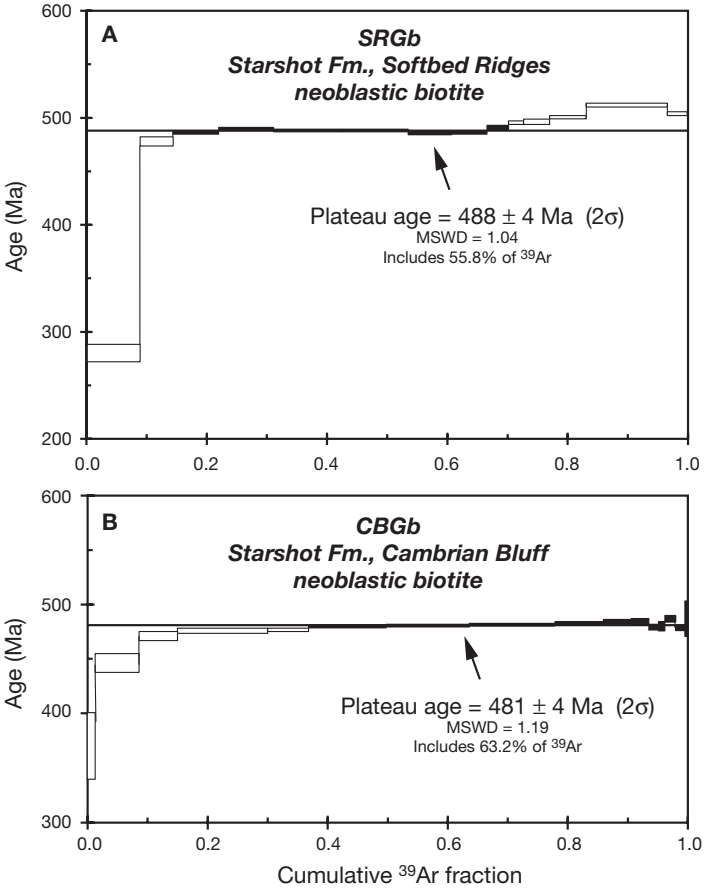


Figure 11. Ar release spectra from step-heating analyses of neoblastic biotites separated from Starshot Formation sandstone at Softbed Ridges and Cambrian Bluff (Fig. 2). Biotite is texturally fine-grained and evenly distributed in the sandstones and is interpreted as formed during greenschist-facies regional metamorphism associated with the Ross Orogeny. Plateau ages assigned for the steps indicated in black. A: Sample SRGb yielded a plateau age of 488 ± 4 Ma (2σ error). B: Sample CBGb yielded a plateau age of 481 ± 4 Ma (2σ error).

5 Ma). We interpret the age obtained from the slate chips as an in situ metamorphic age because the chips most likely have an origin as shale intraclasts. The age of ca. 490 Ma therefore dates the maximum age of metamorphic recrystallization for CBGs1 during incipient growth of slaty minerals.

Coherent, laminated black shale (sample CBGs2) was collected from an interval of interbedded Starshot shale, sandstone, and shale-matrix diamictite on top of the ridge overlooking Nimrod Glacier at the east end of Cambrian Bluff. The release spectrum from this sample is also sigmoidal (Fig. 10B), with the low-temperature steps reflecting Ar loss and the high-temperature steps affected by outgassing of coarser detrital micas. The age spectrum includes a five-step age plateau (representing 52% of the $^{39}$Ar released) with a weighted mean age of 485 ± 4 Ma. Assuming minimal recoil loss of $^{39}$Ar, we interpret the age of ca. 485 Ma as approximating the maximum age of metamorphic crystallization. The $^{40}$Ar/$^{39}$Ar ages for slate formation in the Starshot Formation therefore suggest deformation and low-grade metamorphism of these rocks by earliest Ordovician time.

$^{40}$Ar/$^{39}$Ar step-heating ages were also determined for neoblastic biotite from two of the Starshot sandstone samples for which detrital minerals were dated, at Softbed Ridges (SRGb) and Cambrian Bluff (CBGb). The results are listed in Table 6 and shown in Figure 11. Sample SRGb yielded a slightly discordant age spectrum (Fig. 11A), but with a plateau age of 488 ± 4 Ma (representing 56% of the $^{39}$Ar released). Sample CBGb gave a well-defined plateau from 11 increments (Fig. 11B), representing 63% of the $^{39}$Ar released and yielding an age of 481 ± 4 Ma. Together, these ages indicate that Starshot strata in the region experienced biotite-zone metamorphism prior to ca. 490 and 480 Ma, constraining deposition to earliest Ordovician or older. Biotite-zone metamorphism in these rocks was associated with a combination of late orogenic deformation and regional magmatic heating (e.g., Goodge, 1997).

## DISCUSSION

### Zircon and Muscovite Provenance

Compared to ages of detrital zircon, the detrital muscovites in the Starshot Formation sandstones are uniformly young (580–480 Ma), indicating a proximal provenance with a dominant young source cooling age. Overlap between the youngest apparent ages of detrital muscovite and crystallization ages of nearby igneous intrusions could be interpreted as indicating thermal overprinting of the younger muscovite grains. However, it has been demonstrated that detrital muscovites remain closed systems for argon diffusion even under mid-greenschist facies conditions (e.g., Dunlap et al., 1991). As there is evidence that some grains have undergone variable alteration (CBGm grain 2; DSGm grain 1), it is more likely that the younger muscovite ages result from minor argon loss (<5%) caused by alteration and/or deformation processes. Omitting the analyses of muscovites that were altered or thermally overprinted yields an age distribution with a major peak at ca. 515 Ma (Fig. 12), composed of discrete subpeaks at 509 ± 3 and 518 ± 2 Ma that were contributed by younger and older grains, respectively. Within a given sample, however, the detrital muscovite cooling ages have a much smaller range. In contrast to detrital zircon, none of the detrital muscovites in the Starshot samples predates igneous and metamorphic rocks associated with the Ross Orogen (≤540 Ma). Further, most of the Ross-age detrital zircon is older than most of the muscovite (Fig. 12). Both minerals have age distributions skewed toward young ages and tailing toward old, but the maxima are offset by ~40 m.y. The difference between the muscovite and zircon age distributions is attributable to several factors: (a) muscovite is less robust mechanically than zircon and has a shorter average lifetime during long-distance transport or recycling (Kowalewski and Rimstidt, 2003); (b) muscovite is less robust chemically than zircon and can be altered by prolonged weathering (Goldich, 1938; Robertson and Eggleton, 1991; Elliott et al., 1997; Kowalewski and Rimstidt, 2003); and (c) muscovite, having a lower closure temperature than zircon, is more susceptible to isotopic resetting. Therefore, erosion of a thermally modified, polyphase metamorphic terrain, such as the nearby Nimrod Group, could yield zircons with a wide range of ages but muscovites with Ar cooling ages that are younger than the last metamorphic event that reset older muscovites or that caused growth of new muscovites (e.g., Goodge et al., 1993b; Goodge and Dallmeyer, 1992, 1996; Goodge and Fanning, 1999; Goodge et al., 2001).

A notable observation is that the detrital muscovite ages, within individual samples, are bimodal (Fig. 8). This age bimodality supports the interpretation that there is a mix of variably altered grains within each sample, with the older results representing source ages and the younger ages attributable to alteration-induced argon loss. If all grains had suffered partial Ar loss, a continuum of ages would be expected. Because there are no detrital muscovite grains with ages older than known Ross events, in contrast to detrital zircons, we interpret them as discrete populations of detrital muscovite with a source in the Ross Orogen itself. A tendency to bimodality is also seen in the Ross-age detrital muscovite ages from southern Australia (Turner et al., 1996). Given that muscovite is uncommon as a volcanic phase and that most of the Granite Harbour intrusives contain biotite and/or hornblende, the primary source of detrital muscovite is most likely to be older high-grade metamorphic rocks of the orogen (Nimrod Group or equivalent basement). The presence of minor tourmaline grains in the Starshot and Douglas formations is consistent with the erosion of nearby Granite Harbour plutons, the peraluminous phases of which contain tourmaline (Gunner, 1976; Borg et al. 1990) and pelitic units of the amphibolite-facies Nimrod Group.

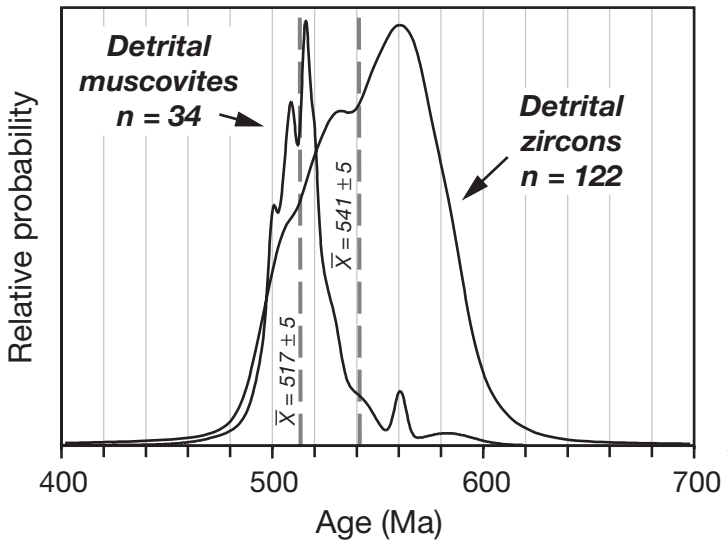


Figure 12. Relative probability distribution of detrital zircon and muscovite ages obtained from the Starshot and Douglas formations, restricted to grains ≤600 Ma and excluding those muscovites interpreted to be affected by thermal resetting between 490–480 Ma. Weighted means of the two populations indicated by dashed dark gray bars. Note the similar form of the age distributions obtained for zircon and muscovite, with a steep curve toward the probability maximum followed by a trailing curve toward younger ages. The zircon distribution appears smoother because of a larger sample set. The two populations are offset by ~24–40 m.y., as indicated by the weighted means and maxima in the distributions.

### Tectonic Implications

Our present understanding of the timing of depositional, deformational, igneous, and metamorphic events pertaining to the upper Byrd Group in the central Transantarctic Mountains is illustrated in Figure 13. Stratigraphic evidence from the Holyoake Range indicates that siliciclastic deposition in response to the onset of Ross deformation commenced ca. 515 Ma (Myrow et al., 2002b). Although supracrustal deformation in the region is diachronous (Rowell et al., 1992; Goodge et al., 1993b; Goodge, 1997; Encarnación et al., 1999), this phase of tectonic

TABLE 6. $^{40}AR/^{39}AR$ STEP-HEATING RESULTS FOR NEOBLASTIC BIOTITE, STARSHOT FORMATION, UPPER BYRD GROUP, ANTARCTICA

| Temp (°C) | Cum $^{39}Ar$ | $^{40}Ar/^{39}Ar$ | $^{37}Ar/^{39}Ar$ | $^{36}Ar/^{39}Ar$ | Vol. $^{39}Ar$ $\times10^{-15}$mol | %Rad. $^{40}Ar$ | Ca/K | $^{40}Ar^*/^{39}Ar$ | Age (Ma) | ± 1s.d. (Ma) |
|---|---|---|---|---|---|---|---|---|---|---|
| SRGb (98-210) Biotite Mass = 0.38 mg; J-value = 0.009429 ± 0.000028 | | | | | | | | | | |
| 700 | 0.0879 | 80.77 | 0.1834 | 0.2125 | 4.305 | 22.2 | 0.3490 | 17.97 | 282.4 | 8.2 |
| 725 | 0.1434 | 55.63 | 0.2296 | 0.0793 | 2.716 | 57.8 | 0.4360 | 32.17 | 477.9 | 4.2 |
| 750 | 0.2188 | 38.18 | 0.1105 | 0.0181 | 3.696 | 86.0 | 0.2100 | 32.81 | 486.3 | 1.7 |
| 775 | 0.3108 | 34.21 | 0.0279 | 0.0038 | 4.504 | 96.6 | 0.0530 | 33.06 | 489.5 | 1.3 |
| 800 | 0.4236 | 33.72 | 0.0056 | 0.0025 | 5.525 | 97.7 | 0.0106 | 32.96 | 488.2 | 1.4 |
| 825 | 0.5347 | 33.70 | 0.0008 | 0.0024 | 5.437 | 97.8 | 0.0015 | 32.95 | 488.1 | 1.1 |
| 850 | 0.6062 | 33.38 | 0.0027 | 0.0019 | 3.502 | 98.2 | 0.0051 | 32.79 | 486.0 | 1.8 |
| 875 | 0.6655 | 33.35 | 0.0030 | 0.0017 | 2.903 | 98.4 | 0.0056 | 32.83 | 486.6 | 1.8 |
| 900 | 0.7015 | 33.84 | 0.0036 | 0.0022 | 1.765 | 98.0 | 0.0068 | 33.16 | 490.8 | 2.1 |
| 925 | 0.7265 | 34.58 | 0.0026 | 0.0036 | 1.226 | 96.9 | 0.0050 | 33.50 | 495.3 | 1.5 |
| 950 | 0.7693 | 34.63 | 0.0078 | 0.0036 | 2.094 | 96.9 | 0.0149 | 33.56 | 496.0 | 2.4 |
| 1000 | 0.8305 | 34.79 | 0.0065 | 0.0030 | 2.998 | 97.4 | 0.0124 | 33.90 | 500.4 | 1.5 |
| 1100 | 0.9647 | 35.41 | 0.0056 | 0.0021 | 6.569 | 98.2 | 0.0105 | 34.77 | 511.6 | 1.6 |
| 1250 | 0.9976 | 37.27 | 0.1123 | 0.0105 | 1.612 | 91.6 | 0.2130 | 34.15 | 503.6 | 2.0 |
| 1400 | 1.0000 | 119.8 | 1.6301 | 0.3460 | 0.118 | 14.8 | 3.1000 | 17.76 | 279.3 | 46.7 |
| Total | | 40.09 | 0.0502 | 0.0276 | 48.97 | | | 31.93 | 474.7 | 2.4 |
| CBGb (98-233A) Biotite Mass = 0.43 mg; J-value = 0.009445 ± 0.000028 | | | | | | | | | | |
| 700 | 0.0129 | 214.9 | 0.0123 | 0.6450 | 1.131 | 11.3 | 0.0233 | 24.17 | 371.0 | 30.2 |
| 730 | 0.0861 | 113.1 | 0.0174 | 0.2819 | 6.442 | 26.3 | 0.0330 | 29.71 | 446.2 | 8.7 |
| 750 | 0.1507 | 68.19 | 0.0193 | 0.1239 | 5.690 | 46.3 | 0.0367 | 31.55 | 470.6 | 4.2 |
| 775 | 0.3007 | 43.40 | 0.0119 | 0.0387 | 13.19 | 73.6 | 0.0226 | 31.92 | 475.4 | 2.2 |
| 800 | 0.3684 | 33.97 | 0.0095 | 0.0066 | 5.964 | 94.2 | 0.0181 | 31.99 | 476.3 | 1.4 |
| 825 | 0.4973 | 32.63 | 0.0049 | 0.0013 | 11.34 | 98.7 | 0.0093 | 32.23 | 479.4 | 1.3 |
| 850 | 0.6366 | 32.58 | 0.0021 | 0.0009 | 12.26 | 99.1 | 0.0039 | 32.27 | 480.0 | 1.3 |
| 875 | 0.7794 | 32.65 | 0.0001 | 0.0009 | 12.57 | 99.1 | 0.0001 | 32.35 | 481.0 | 1.2 |
| 900 | 0.8592 | 32.86 | 0.0001 | 0.0013 | 7.021 | 98.7 | 0.0001 | 32.43 | 482.1 | 1.6 |
| 925 | 0.9068 | 33.48 | 0.0001 | 0.0030 | 4.185 | 97.3 | 0.0002 | 32.57 | 483.8 | 2.0 |
| 950 | 0.9358 | 33.79 | 0.0034 | 0.0041 | 2.557 | 96.3 | 0.0064 | 32.54 | 483.5 | 2.8 |
| 975 | 0.9517 | 34.93 | 0.0006 | 0.0092 | 1.391 | 92.1 | 0.0011 | 32.17 | 478.7 | 2.7 |
| 1000 | 0.9628 | 35.38 | 0.0038 | 0.0106 | 0.978 | 91.1 | 0.0072 | 32.23 | 479.4 | 4.3 |
| 1050 | 0.9806 | 35.22 | 0.0003 | 0.0082 | 1.594 | 93.0 | 0.0005 | 32.76 | 486.3 | 3.0 |
| 1100 | 0.9961 | 35.46 | 0.0043 | 0.0112 | 1.335 | 90.6 | 0.0082 | 32.12 | 478.0 | 2.4 |
| 1250 | 0.9989 | 57.54 | 0.0377 | 0.0836 | 0.255 | 57.0 | 0.0715 | 32.78 | 486.6 | 16.1 |
| 1400 | 1.0000 | 336.6 | 0.0081 | 1.0789 | 0.093 | 5.3 | 0.0154 | 17.74 | 279.5 | 147.1 |
| Total | | 45.50 | 0.0064 | 0.0459 | 88.0 | | | 31.89 | 475.0 | 2.9 |

*Note*: 1. Errors are 1σ uncertainties and exclude uncertainties in the J-value. 2. Data are corrected for mass spectrometer backgrounds, discrimination and radioactive decay. 3. Interference corrections: $(^{36}Ar/^{37}Ar)_{Ca}$ = 3.2E-4; $(^{39}Ar/^{37}Ar)_{Ca}$ = 7.86E-4; $(^{40}Ar/^{39}Ar)_{K}$ = 3.50E-2. 4. J-value is based on an age of 98.8 Ma for GA-1550 biotite.

movement, which is biostratigraphically well-constrained, is the earliest documented along the length of the orogen in Antarctica. Detrital mineral ages from throughout the group record molasse deposition over a period of at least 25 m.y. from Botomian to Early Ordovician time. Weighted mean ages of discrete detrital muscovite populations provide the best constraint for maximum depositional age of the Starshot samples that we analyzed, which are estimated to be between ca. 520 and 505 Ma (or middle Early Cambrian to late Middle Cambrian). In other areas of the Transantarctic Mountains, deposition persisted to Early Ordovician time (Fig. 13; Goodge et al., 2002). Combining the maximum depositional age of 515 Ma with constraints from crosscutting igneous units (≤508 Ma) and metamorphic cooling ages (≤492 Ma) discussed here yields a maximum period of sedimentation of between 7 and 25 m.y. (Fig. 13). Within the framework allowed by these biostratigraphic and crosscutting age constraints, the unimodal, young populations of detrital zircon and muscovite thus show that there was only a short time interval between formation of the youngest source rocks, regional deformation, and late-orogenic igneous intrusion, suggesting rapid erosion and short transport distances.

Age data from geographically separated areas show that deposition was regionally diachronous and that events were more closely spaced in certain areas. For example, ages of crosscutting igneous units at Softbed Ridges and Cambrian Bluff indicate that deposition of sediment in those areas ended no later than ca. 500 and 489 Ma, respectively. Likewise, $^{40}Ar/^{39}Ar$ ages from metamorphic slate and biotite in these areas restrict deposition to older than ca. 484 and 488 Ma, respectively. The post-depositional age constraints indicate that the Starshot Formation in these two areas is earliest Ordovician or older, yet comparing the mean detrital muscovite ages with the crosscutting age constraints also provides an estimate for the duration of sedimentation. In the Softbed Ridges area, detrital muscovite cooling ages and the

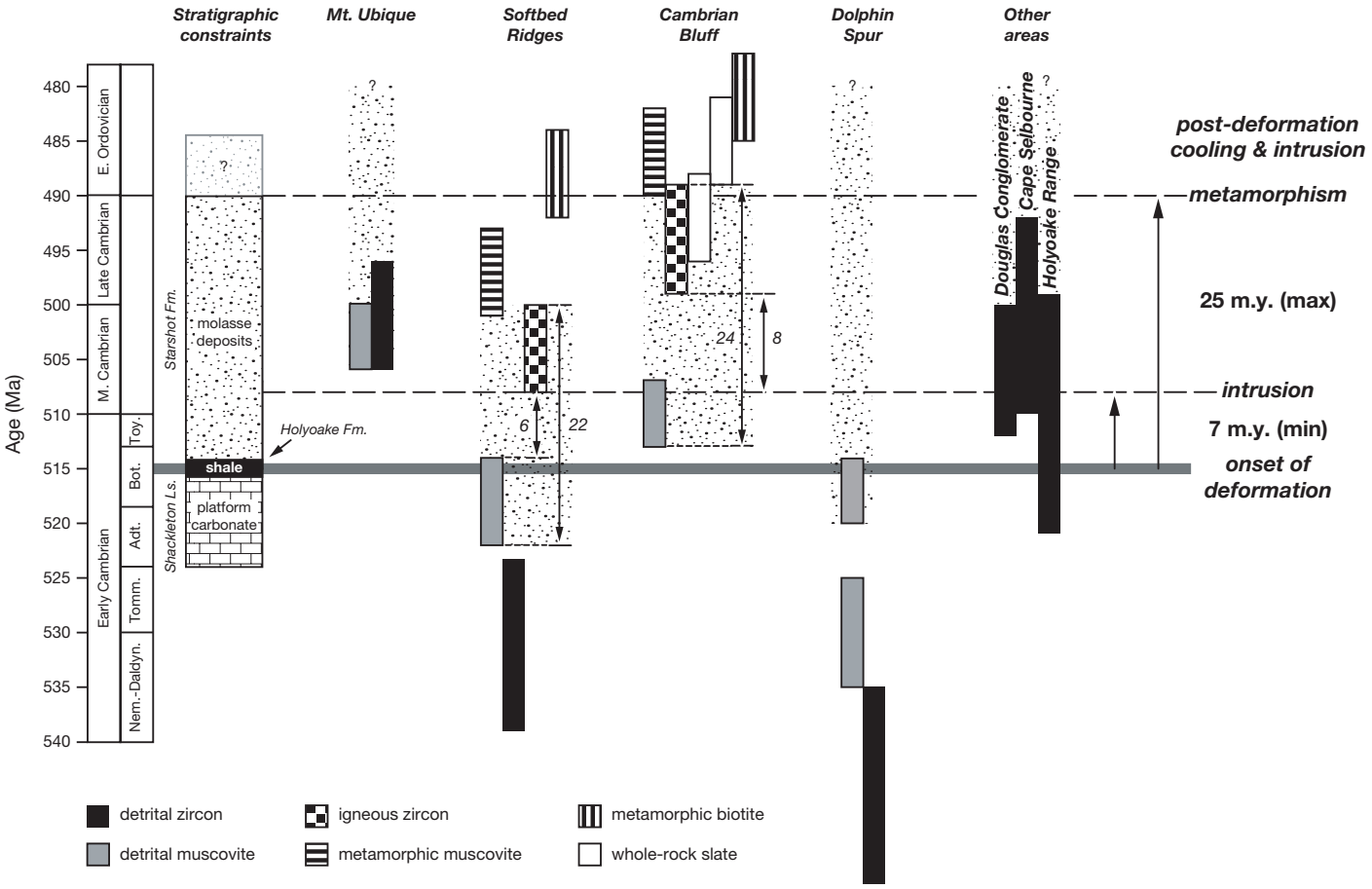


Figure 13. Diagram summarizing available age constraints on the timing of upper Byrd Group siliciclastic deposition in the areas discussed in text. General stratigraphic constraints as shown in Figure 3. Onset of siliciclastic deposition marked by shale of Holyoake Formation, at ca. 515 Ma (Myrow et al., 2002b), followed by molasse deposits of Starshot Formation; initial deposition related to a contractional pulse of supracrustal deformation in the region. Synorogenic deposition is also recorded by carbonate-clast conglomerate of the Douglas Conglomerate, but not shown here. Youngest populations (including weighted mean ages and uncertainties) of detrital zircon and muscovite from Starshot sandstone samples are indicated by black and gray bars, respectively. Texturally coarse muscovite with younger ages interpreted as a result of thermal resetting (horizontal ruling). Also shown are ages of crosscutting igneous rocks (checkerboard), metamorphic slate ages (white), and ages of neoblastic biotite (vertical ruling), which indicate the timing of post-deformation cooling and intrusion. Horizontal dashed lines indicate likely minimum and maximum durations, 7 and 25 m.y. respectively, of molasse deposition in the upper Byrd Group forearc basin, as constrained by the detrital mineral and post-depositional ages shown. Age data from individual areas differ (as shown by brackets for Softbed Ridges and Cambrian Bluff areas), constrained by crosscutting relationships and post-depositional metamorphic growth; range of possible deposition ages in each area indicated by stipple pattern. Detrital zircon data from other Byrd Group units (Douglas Conglomerate and Dick Formation) suggest deposition continued regionally into the Ordovician.

age of crosscutting gabbro bodies restrict sedimentation to 6–22 m.y., depending on treatment of uncertainties (Fig. 13). For the Starshot Formation in the area of Cambrian Bluff, the detrital muscovite and aplite dike ages similarly restrict deposition to an 8–24 m.y. period. More data will refine these estimates, but it can already be concluded that individual units within the molasse succession were deposited relatively rapidly.

It appears, therefore, that siliciclastic deposition was triggered soon after the onset of regional deformation and that it occurred in brief pulses over a period of up to 7–25 m.y. Recent studies in the Ross Orogen show that most of the siliciclastic material previously assumed to be Neoproterozoic in age is in fact syn- to late-orogenic (Millar and Storey, 1995; Ireland et al., 1998; Rowell et al., 2001; Goodge et al., 2002). By applying different mineral chronometers, the upper Byrd Group sandstone units document a short time lag of only a few million years between onset of deformation and active erosion. A similar conclusion was reached by Turner et al. (1996), who found that Ar-Ar ages of detrital muscovites in the early Paleozoic flysch of southeastern Australia are indistinguishable from their deposition ages (505–485 Ma), implying that the flysch was deposited at essentially the same time that the sediment source, the Ross-Delamerian orogen, was exhumed, and that exhumation was extremely rapid (5–15 mm/yr).

Rapid sedimentary response to tectonism is well documented in other, younger orogenic belts. In the modern Hima-

laya, detrital zircons obtained from the contemporary Indus River yield fission-track ages of only a few million years (Cerveny et al., 1988). Furthermore, Siwalik Group sandstones in the Himalayas contain zircons that were only a few million years old at the time of deposition, suggesting that high denudation rates were maintained since 18 Ma. Likewise, Early Cretaceous forearc deposits in Baja California reflect rapid unroofing of the Peninsular Ranges batholith and its associated arc basement rocks in a continental-margin setting (Busby et al., 1998; Kimbrough et al., 2001). Here, stratigraphic and geochronological data document denudation rates of ~1 mm/yr that are related to intra-arc deformation and magmatism, which in turn yielded forearc sedimentation rates of 1000 m/m.y. over a 10–15 m.y. period. A short time lag between the age of the principal source rocks in the Peninsular Ranges and the age of deposition implies that erosion and rapid forearc sedimentary accumulation rates were driven by a combination of tectonic and magmatic intra-arc thickening. Similar linkages were inferred for the Sierra Nevada–Great Valley arc-forearc system (Linn et al., 1992).

The detrital mineral ages and the ages of crosscutting or overprinting events limits the exhumation history of the igneous and metamorphic source rocks, as well as subsequent molasse deposition, to a short time period. This suggests rapid denudation rates, which can be evaluated by comparing discordant cooling ages obtained from different mineral chronometers. Although this approach is applicable in some sedimentary systems, in this case we cannot be certain of the specific geological source or crustal level from which the detrital minerals were derived. Regional orogenic cooling rates can be obtained, however, from the adjacent crystalline basement. U-Pb and $^{40}Ar/^{39}Ar$ cooling ages from different mineral chronometers in the Nimrod Group yielded a post-kinematic cooling rate of ~10 °C/m.y. for igneous and metamorphic rocks of the middle crust (Goodge and Dallmeyer, 1992, 1996). Using a metamorphic geotherm of ~25 °C/km, this inverts to a denudation rate of ~0.4 mm/yr, comparable in order of magnitude to modern convergent or collision belts (e.g., Harrison et al., 1992). For example, recent exhumation rates of 0.2–1.0 mm/yr are reported from the Himalayan, Alpine, and Andean orogenic belts (Zeitler 1985; Copeland et al., 1987; Burbank and Beck, 1991; Harrison et al., 1992; Gregory-Wodzicki, 2000; Bernet et al., 2001; White et al., 2002). By comparison, exhumation rates of 5–15 mm/yr proposed for the Ross-Delamerian orogen in South Australia (Turner et al., 1996) are extreme. Rapid unroofing in the axial Ross Orogen is consistent with the sharp stratigraphic transition observed within the upper Byrd Group of the Holyoake Range, which reflects severe syntectonic erosion, development of an unconformity on uplifted carbonate, and outpouring of clastic materials into marginal-marine molasse basins (Myrow et al., 2002b).

If we estimated cooling rates using zircon and muscovite as detrital mineral chronometers, we would obtain values on the order of 10–30 °C/m.y., which are similar to cooling rates determined for the Nimrod Group and which imply similar denudation rates using the basement geotherm. If the muscovite ages are partially reset and the detrital sources are actually older, or if the geotherm were cooler, the resulting denudation rates would be even faster. Cooling rates calculated from detrital mineral closure ages are highly dependent on grain-age sampling bias, assumed closure temperature, and determination that the minerals were derived from the same source rocks, among other factors. Having at present only two detrital mineral chronometers of uncertain specific source relationship is therefore insufficient to uniquely define cooling rates, but it is likely that there is a link between the basement and supracrustal successions with respect to uplift, cooling, denudation, and sedimentation. Additional detrital mineral age data (e.g., amphibole, feldspar, apatite, etc.) would provide additional constraints for the inferred denudation rates.

## CONCLUSIONS

We argue that siliciclastic rocks of the upper Byrd Group represent a depositional response to rapid denudation in the developing Ross Orogen. These rocks are interpreted as forearc molasse deposits on the basis of their sedimentary structures, composition, transport direction, and provenance. In the context of regional tectonic relationships, they represent an "unroofing" succession, in which igneous and metamorphic rocks of the Ross magmatic arc, as well as older, structurally shortened passive-margin deposits, were erosionally inverted and deposited in forearc marginal basins. The entire episode of interrelated tectonism, denudation, sedimentation, deformation, and magmatism appears to have lasted for a period of 7–25 m.y. in the late Early Cambrian to earliest Ordovician. Along with evidence of left-oblique transpression along the Ross margin (Goodge et al., 1993a), the timing constraints indicate both erosional and tectonic controls on denudation. Because the short lag time between tectonism and sedimentation, as deduced from the available geochronological constraints, indicates a rapid denudational response to the orogenic process, crustal thickening produced by both magmatic intrusion and structural shortening appears to have been balanced in part by erosional exhumation.

## ACKNOWLEDGMENTS

Field and laboratory work were supported by the National Science Foundation (OPP-9725426 and OPP-9912081). We thank the ANU Electron Microscopy Unit for assistance with CL imaging, and Shane Paxton, John Mya, and Sally Mussett for their excellent mineral separations. We also thank Keiji Miswa (NIPR) for assistance in collecting the SHRIMP U-Pb data. We are grateful for critical reviews by Matt Heizler and John Miller, who provided helpful insight that reshaped our interpretations.

## REFERENCES CITED

Allibone, A., and Wysoczanski, R.J., 2002, Initiation of magmatism during the Cambro-Ordovician Ross Orogeny in southern Victoria Land, Antarctica: Geological Society of America Bulletin, v. 114, p. 1007–1018.

Allibone, A.H., Cox, S.C., and Smillie, R.W., 1993, Granitoids of the Dry Val-

leys area, southern Victoria Land: geochemistry and evolution along the early Palaeozoic Antarctic craton margin: New Zealand Journal of Geology and Geophysics, v. 36, p. 299–316.

Armienti, P., Ghezzo, C., Innocenti, F., Manetti, P., Rocchi, S., and Tonarini, S., 1990, Isotope geochemistry and petrology of granitoid suites from Granite Harbour Intrusives of the Wilson Terrane, North Victoria Land, Antarctica: European Journal of Mineralogy, v. 2, p. 103–123.

Armstrong, R., De Wit, M.J., Reid, D., York, D. and Zartman, R., 1998, Cape Town's Table Mountain reveals rapid Pan-African uplift of its basement rocks: Journal of African Earth Sciences, v. 27, no. 1A, p. 10–11.

Bernet, M., Zattin, M., Garver, J.I., Brandon, M.T., and Vance, J.A., 2001, Steady-state exhumation of the European Alps: Geology, v. 29, p. 35–38.

Borg, S.G., Stump, E., Chappell, B.W., McCulloch, M.T., Wyborn, D., Armstrong, R.L., and Holloway, J.R., 1987, Granitoids of northern Victoria Land, Antarctica: Implications of chemical and isotopic variations to regional crustal structure and tectonics: American Journal of Science, v. 287, p. 127–169.

Borg, S.G., DePaolo, D.J., and Smith, B.M., 1990, Isotopic structure and tectonics of the central Transantarctic Mountains: Journal of Geophysical Research, v. 95, p. 6647–6669.

Burbank, D.W., and Beck, R.A., 1991, Rapid, long-term rates of denudation: Geology, v. 19, p. 1169–1172.

Busby, C.J., Smith, D., Morris, W., and Fackler-Adams, B.N., 1998, Evolutionary model for convergent margins facing large ocean basins; Mesozoic Baja California, Mexico: Geology, v. 26, p. 227–230.

Cerveny, P.F., Naeser, N.D., Zeitler, P.K., Naeser, C.W., and Johnson, N.M., 1988, History of uplift and relief of the Himalaya during the past 18 million years: evidence from fission-track ages of detrital zircons from sandstones of the Siwalik Group, *in* Kleinspehn, K.L., and Paola, C., eds., New Perspectives in Basin Analysis: New York, Springer-Verlag, p. 43–61.

Compston, W., Williams, I.S., Kirschvink, J.L., Zhang, Z., and Ma, G., 1992, Zircon U-Pb ages for the Early Cambrian time-scale: Journal of the Geological Society of London, v. 149, p. 171–184.

Copeland, P., and Harrison, T.M., 1990, Episodic rapid uplift in the Himalaya revealed by $^{40}Ar/^{39}Ar$ analysis of detrital K-feldspar and muscovite, Bengal fan: Geology, v. 18, p. 354–357.

Copeland, P., Harrison, T.M., Kidd, W.S.F., Ronghua, X., and Yuquan, Z., 1987, Rapid early Miocene acceleration of uplift in the Gangdese Belt, Xizang (southern Tibet), and its bearing on accommodation mechanisms of the India-Asia collision: Earth and Planetary Science Letters, v. 86, p. 240–252.

Cox, S.C., Parkinson, D.L., Allibone, A.H., and Cooper, A.F., 2000, Isotopic character of Cambro-Ordovician plutonism, southern Victoria Land, Antarctica: New Zealand Journal of Geology and Geophysics, v. 43, p. 501–520.

Dunlap, W.J., Teyssier, C., McDougall, I. and Baldwin, S., 1991, Ages of deformation from K/Ar and $^{40}Ar/^{39}Ar$ dating of white micas: Geology, v. 19, p. 1213–1216.

Elliott, W.C., Savin, S.M., Dong, H. and Peacor, D.R., 1997, A paleoclimate interpretation derived from pedogenic clay minerals from the Piedmont Province, Virginia: Chemical Geology, v. 142, no. 3–4, p. 201–211.

Encarnación, J., Rowell, A.J., and Grunow, A.M., 1999, A U-Pb age for the Cambrian Taylor Formation, Antarctica: Implications for the Cambrian time scale: Journal of Geology, v. 107, no. 4, p. 497–504.

Fergusson, C.L., and Phillips, D., 2001, $^{40}Ar/^{39}Ar$ and K-Ar age constraints on the timing of regional deformation, south coast of New South Wales, Lachlan Fold Belt: problems and implications: Australian Journal of Earth Sciences, v. 48, p. 395–408.

Fitzsimons, I.C.W., 2000, A review of tectonic events in the East Antarctic Shield, and their implications for Gondwana and earlier supercontinents: Journal of African Earth Sciences, v. 31, no. 1, p. 3–23.

Flöttmann, T., James, P., Rogers, J., and Johnson, T., 1994, Early Palaeozoic foreland thrusting and basin reactivation at the Palaeo-Pacific margin of the southeastern Australian Precambrian Craton: a reappraisal of the structural evolution of the Southern Adelaide Fold-Thrust Belt: Tectonophysics, v. 234, p. 95–116.

Garver, J.I., Brandon, M.T., Roden-Tice, M., and Kamp, P.J.J., 1999, Exhumation history of orogenic highlands determined by detrital fission-track thermochronology, *in* Ring, U., Brandon, M.T., Lister, G.S., and Willett, S.D., eds., Exhumation Processes: Normal Faulting, Ductile Flow and Erosion: London, Geological Society Special Publication 154, p. 283–304.

Goldich, S.S., 1938, A study in rock weathering: Journal of Geology, v. 46, p. 17–58.

Goodge, J.W., 1997, Latest Neoproterozoic basin inversion of the Beardmore Group, central Transantarctic Mountains, Antarctica: Tectonics, v. 16, no. 4, p. 682–701.

Goodge, J.W., and Dallmeyer, R.D., 1992, $^{40}Ar/^{39}Ar$ mineral age constraints on the Paleozoic tectonothermal evolution of high-grade basement rocks within the Ross orogen, central Transantarctic Mountains: Journal of Geology, v. 100, p. 91–106.

Goodge, J.W., and Dallmeyer, R.D., 1996, Contrasting thermal evolution within the Ross Orogen, Antarctica: Evidence from mineral $^{40}Ar/^{39}Ar$ ages: Journal of Geology, v. 104, p. 435–458.

Goodge, J.W., and Fanning, C.M., 1999, 2.5 billion years of punctuated Earth history as recorded in a single rock: Geology, v. 27, p. 1007–1010.

Goodge, J.W., Hansen, V.L., Peacock, S.M., Smith, B.K., and Walker, N.W., 1993a, Kinematic evolution of the Miller Range shear zone, central Transantarctic Mountains, Antarctica, and implications for Neoproterozoic to early Paleozoic tectonics of the East Antarctic margin of Gondwana: Tectonics, v. 12, no. 6, p. 1460–1478.

Goodge, J.W., Walker, N.W., and Hansen, V.L., 1993b, Neoproterozoic-Cambrian basement-involved orogenesis within the Antarctic margin of Gondwana: Geology, v. 21, p. 37–40.

Goodge, J.W., Fanning, C.M., and Bennett, V.C., 2001, U-Pb evidence of ~1.7 Ga crustal tectonism during the Nimrod Orogeny in the Transantarctic Mountains, Antarctica: Implications for Proterozoic plate reconstructions: Precambrian Research, v. 112, p. 261–288.

Goodge, J.W., Myrow, P., Williams, I.S., and Bowring, S., 2002, Age and provenance of the Beardmore Group, Antarctica: Constraints on Rodinia supercontinent breakup: Journal of Geology, v. 110, p. 393–406.

Goodge, J.W., Williams, I.S., and Myrow, P., 2004, Provenance of Neoproterozoic and lower Paleozoic siliciclastic rocks of the central Ross Orogen, Antarctica: Detrital record of rift-, passive-, and active-margin sedimentation: Geological Society of America Bulletin (in press).

Gregory-Wodzicki, K.M., 2000, Uplift history of the Central and Northern Andes: A review: Geological Society of America Bulletin, v. 112, p. 1091–1105.

Gunner, J.D., 1976, Isotopic and geochemical studies of the pre-Devonian basement complex, Beardmore Glacier region, Antarctica: Ohio State University, Institute of Polar Studies Report No. 41, 126 p.

Harrison, T.M., Copeland, P., Kidd, W.S.F., and Yin, A., 1992, Raising Tibet: Science, v. 255, p. 1663–1670.

Ireland, T.R. and Gibson, G.M., 1998, SHRIMP monazite and zircon geochronology of high-grade metamorphism in New Zealand: Journal of Metamorphic Geology, v. 16, no. 2, p. 149–167.

Ireland, T.R., Flöttmann, T., Fanning, C.M., Gibson, G.M., and Preiss, W.V., 1998, Development of the early Paleozoic Pacific margin of Gondwana from detrital-zircon ages across the Delamerian orogen: Geology, v. 26, p. 243–246.

Kimbrough, D.L., Smith, D.P., Mahoney, J.B., Moore, T.E., Grove, M., Gastil, R.G., Ortega-Rivera, A., and Fanning, C.M., 2001, Forearc-basin sedimentary response to rapid Late Cretaceous batholith emplacement in the Peninsular Ranges of southern and Baja California: Geology, v. 29, p. 491–494.

Kowalewski, M., and Rimstidt, J.D., 2003, Average lifetime and age spectra of detrital grains: toward a unifying theory of sedimentary particles: Journal of Geology, v. 111, no. 4, p. 427–440.

Laird, M.G., 1981, Lower Paleozoic rocks of the Ross Sea area and their significance in the Gondwana context: Journal of the Royal Society of New Zealand, v. 11, no. 4, p. 425–438.

Laird, M.G., 1991, The Late Proterozoic-Middle Paleozoic rocks of Antarctica, *in* Tingey, R.J., ed., The geology of Antarctica: Oxford monograph on geology and geophysics: Oxford, UK, Clarendon Press, p. 74–119.

Laird, M.G., Mansergh, G.D., and Chappell, J.M.A., 1971, Geology of the central Nimrod Glacier area, Antarctica: New Zealand Journal of Geology and Geophysics, v. 14, p. 427–468.

Linn, A.M., DePaolo, D.J., and Ingersoll, R.V., 1992, Nd-Sr isotopic, geochemical, and petrographic stratigraphy and paleotectonic analysis: Mesozoic Great Valley forearc sedimentary rocks of California: Geological Society of America Bulletin, v. 104, p. 1264–1279.

Ludwig, K.R., 1999, Using Isoplot/Ex, Version 2.01: a geochronological toolkit for Microsoft Excel: Berkeley Geochronology Center Special Publication 1a, 47 p.

Ludwig, K.R., 2000, SQUID 1.00—A User's Manual: Berkeley Geochronology Center Special Publication 2, 17 p.

McDougall, I., and Feibel, C.S., 1999, Numerical age control for the Miocene-Pliocene succession at Lothagam, a hominoid-bearing sequence in the northern Kenya Rift: Journal of the Geological Society of London, v. 156, p. 731–745.

McDougall, I., and Harrison, T.M., 1999, Geochronology and thermochronology by the $^{40}Ar/^{39}Ar$ method (2nd ed.): New York, Oxford University Press, 282 p.

Millar, I.A., and Storey, B.C., 1995, Early Palaeozoic rather than Neoproterozoic volcanism and rifting within the Transantarctic Mountains: Journal of the Geological Society of London, v. 152, p. 417–460.

Myrow, P., and Goodge, J.W., 1999, Reinterpretation of depositional and tectonic setting of Neoproterozoic Strata, Transantarctic Mountains, *in* Skinner, D.N.B., ed., Proceedings of 8th International Symposium on Antarctic Earth Sciences: Wellington, New Zealand, p. 222.

Myrow, P.M., Fischer, W., and Goodge, J.W., 2002a, Wave-modified turbidites: Combined-flow shoreline and shelf deposits, Cambrian, Antarctica: Journal of Sedimentary Research, v. 72, no. 5, p. 641–656.

Myrow, P.M., Pope, M.C., Goodge, J.W., Fischer, W., and Palmer, A.R., 2002b, Depositional history of pre-Devonian strata and timing of Ross Orogenic tectonism in the central Transantarctic Mountains, Antarctica: Geological Society of America Bulletin, v. 114, p. 1070–1088.

Oliver, R.L., 1972, Geology of an area near the mouth of Beardmore Glacier, Ross Dependency, *in* Adie, R.J., ed., Antarctic geology and geophysics: Oslo, Universitetsforlaget, p. 379–385.

Paces, J.B., and Miller, J.D., 1993, Precise U-Pb ages of Duluth Complex and related mafic intrusions, northeastern Minnesota: Geochronological insights to physical, petrogenic, paleomagnetic, and tectonomagmatic processes associated with the 1.1 Ga Midcontinent Rift System: Journal of Geophysical Research, v. 98, p. 13,997–14,013.

Preiss, W.V., 2000, The Adelaide Geosyncline of South Australia and its significance in Neoproterozoic continental reconstruction: Precambrian Research, v. 100, no. 1/3, p. 21–63.

Rees, M.N., and Rowell, A.J., 1991, The pre-Devonian Palaeozoic clastics of the central Transantarctic Mountains: Stratigraphy and depositional settings, *in* Thomson, M.R.A., Crame, J.A., and Thomson, J.W., eds., Geological Evolution of Antarctica: New York, Cambridge University Press, p. 187–192.

Renne, P., Swisher, C.C., Deino, A.L., Karner, D.B., Owens, T.L., and DePaolo, D.J., 1998, Intercalibration of standards, absolute ages and uncertainties in $^{40}Ar/^{39}Ar$ dating: Chemical Geology, v. 145, p. 117–152.

Robertson, I.D.M. and Eggleton, R.A., 1991, Weathering of granitic muscovite to kaolinite and halloysite and of plagioclase-derived kaolinite to halloysite: Clays and Clay Minerals, v. 39, no. 2, p. 113–126.

Rocchi, S., Tonarini, S., Armienti, P., Innocenti, F., and Manetti, P., 1997, Geochemical and isotopic structure of the early Palaeozoic active margin of Gondwana in northern Victoria Land, Antarctica: Tectonophysics, v. 284, p. 261–281.

Rowell, A.J., Rees, M.N., Cooper, R.A., and Pratt, B.R., 1988, Early Paleozoic history of the central Transantarctic Mountains: Evidence from the Holyoake Range, Antarctica: New Zealand Journal of Geology and Geophysics, v. 31, p. 397–404.

Rowell, A.J., Rees, M.N., and Evans, K.R., 1992, Evidence of major Middle Cambrian deformation in the Ross orogen, Antarctica: Geology, v. 20, p. 31–34.

Rowell, A.J., van Schmus, W.R., Storey, B.C., Fetter, A.H., and Evans, K.R., 2001, Latest Neoproterozoic to Mid-Cambrian age for the main deformation phases of the Transantarctic Mountains: New stratigraphic and isotopic constraints from the Pensacola Mountains, Antarctica: Journal of Geological Society of London, v. 158, p. 295–308.

Steiger, R.H., and Jäger, E., 1977, Subcommission on geochronology: Convention on the use of decay constants in geo- and cosmochronology: Earth and Planetary Science Letters, v. 36, p. 359–362.

Stump, E., 1995, Ross orogen of the Transantarctic Mountains: New York, Cambridge University Press, 284 p.

Tera, F., and Wasserburg, G.J., 1972, U-Th-Pb systematics in three Apollo 14 basalts and the problem of initial Pb in lunar rocks: Earth and Planetary Science Letters, v. 14, p. 281–304.

Tetley, N., McDougall, I., and Heydegger, H.R., 1980, Thermal neutron interferences in the $^{40}Ar/^{39}Ar$ dating technique: Journal of Geophysical Research, v. 85, p. 7201–7205.

Turner, S.P., Kelley, S.P., VandenBerg, A.H.M., Foden, J.D., Sandiford, M and Flöttmann, T., 1996, Source of the Lachlan fold belt flysch linked to convective removal of the lithospheric mantle and rapid exhumation of the Delamerian-Ross fold belt: Geology, v. 24, p. 941–944.

White, N.M., Pringle, M.S., Garzanti, E., Bickle, M., Najman, Y.M.R., Chapman, H.J., and Friend, P., 2002, Constraints on the exhumation and erosion of the High Himalayan Slab, NW India, from foreland basin deposits: Earth and Planetary Science Letters, v. 195, p. 29–44.

Williams, I.S., 1998, U-Th-Pb geochronology by ion microprobe, *in* McKibben, M.A., Shanks III, W.C., and Ridley, W.I., eds., Applications of microanalytical techniques to understanding mineralizing processes, reviews in economic geology, p. 1–35.

Williams. I.S., Goodge, J., Myrow, P., Burke, K. and Kraus, J., 2002, Large scale sediment dispersal associated with the Late Neoproterozoic assembly of Gondwana: Abstracts of the 16th Australian Geological Convention, v. 67, p. 238.

Zeitler, P.K., 1985, Cooling history of the NW Himalaya, Pakistan: Tectonics, v. 4, no. 1, p. 127–151.

Manuscript Accepted by the Society October 21, 2003